INDUCED CHARGE DISTRIBUTIONS IN PROPORTIONAL DETECTORS

E. MATHIESON

INDUCED CHARGE DISTRIBUTIONS
IN PROPORTIONAL DETECTORS

E. MATHIESON

Although this is a private circulated report, copyright regulations nevertheless apply. Reproduction or photocopying of any part may not be carried out without the written permission of the author.

(Added in proof: It is with great regret we record that the author of this monograph passed away in January 1991, just shortly after its completion. Permission for reproduction or photocopying should be requested from G.C. Smith, Brookhaven National Laboratory, Upton, New York 11973.)

To my wife Margaret

INDUCED CHARGE DISTRIBUTIONS IN PROPORTIONAL DETECTORS

Preface

Contents

Chapter 1. Basic theory and definitions

Chapter 2. Coaxial geometry I.
Basic formulae

Chapter 3. Multiwire geometry I.
Weber approximation

Chapter 4. Multiwire geometry II.
General treatment

Chapter 5. Multiwire geometry III.
Cathode charge distributions

Chapter 6. Parallel plate geometry.
Anode and cathode charge distributions

Chapter 7. Coaxial geometry II.
Cathode charge distributions

Appendices

1. Weber approximation for MWPC potential
2. Derivation of single wire formula
3. Derivation of cathode strip formula
4. Evaluation of exponential integral
5. Evaluation of $H_0(\omega)$ and $H(\omega)$
6. Comments on gas gain formulae
7. Prompt electron signal in wire counters

Preface

This monograph is a collection of methods for calculating induced charge distributions in gas proportional detectors of conventional geometry. These methods have been mainly taken from papers already published, in collaboration with colleagues, by the writer, but there are also additional notes and comments.

The task of gathering together this previously scattered work was originally motivated by the wish for greater convenience; to have the information all in one place. There was also the satisfaction of attempting to arrange material with a common theme in a logical and self-consistent manner. It is hoped, however, that the final result may also be of assistance or interest to younger colleagues working with proportional detectors, and perhaps especially, to research students just encountering them.

Special computer programmes for field calculations are now becoming more widely available, and their use is indeed necessary for tackling irregular geometry, and most three-dimensional, problems. However for conventional geometry detectors the theoretical analysis can usually be carried through to a sufficiently late stage that such special packages become quite unnecessary. The real advantage of employing this more analytical approach, however, is that a fuller, more productive understanding necessarily emerges of detector operation and of the basic physics involved.

It should be stressed that this monograph does not attempt in any way to present a history of wire chambers or proportional detectors. It is only a collection, restricted and specialised, of topics on induced charge calculation. General references have been given to help the reader, and of course previous work directly relevant to the establishment or development of a particular calculation has been acknowledged. However the background history of each topic has not been referenced; this would be inappropriate in a small monograph of such limited aims. If, within these limitations, I have unintentionally omitted to give correct priority to any research work then I apologise to those concerned, and would be grateful to be informed.

Theoretical calculations in isolation are totally barren. It is only in interplay with measurement and observation that they gain any meaning. I am deeply grateful in this respect to my colleagues Dr. G.C. Smith (Brookhaven National Laboratory), Dr. T.J. Harris (Leicester University) and Dr. J.S. Gordon (V.S.W. Sci. Instr.). Their special skills and knowledge have been essential in placing some experimental flesh on my theoretical skeletons.

E. Mathieson Leicester University, England

Contents

Chap.1 Basic theory and definitions
- 1.1 Methods of calculating induced charge
- 1.2 Ion motion
- 1.3 Induced charge and signal charge
- 1.4 Nomenclature
- 1.5 Signal processing
- 1.6 The avalanche charge
- 1.7 Geometry limitations
- References

Chap.2 Coaxial geometry I. Basic formulae.
- 2.1 Formulae for field, potential and capacitance
- 2.2 Anode induced and net charges
- 2.3 Time development of anode charge
- 2.4 Signal processing
- References

Chap.3 Multiwire geometry II. Weber approximation
- 3.1 Introduction
- 3.2 Potential, capacitance and field formulae
  - 3.2.1 Potential distribution. Anode at unit potential
  - 3.2.2 Potential distribution. Cathode at unit potential
  - 3.2.3 Capacitance per unit length of wire
  - 3.2.4 Field formulae
- 3.3 Field lines and ion trajectories
  - 3.3.1 Field line formulae
  - 3.3.2 Ion trajectories
- 3.4 Ion collection times
  - 3.4.1 Average ion collection time
  - 3.4.2 Minimum ion collection time
- 3.5 Anode and cathode charge waveforms
  - 3.5.1 Coaxial region approximation
  - 3.5.2 General case
  - 3.5.3 Dependence of gas gain on alpha
- 3.6 Dependence of gas gain on count rate
- References

Chap.4 Multiwire geometry II. General treatment
- 4.1 Introduction

4.2 Potential and capacitance due to single wire
4.3 Potential, field and capacitance in multiwire chambers
  4.3.1 Potential distribution
  4.3.2 Capacitance per unit length of wire
  4.3.3 Field formulae
  4.3.4 Cathode at finite potential
  4.3.5 Chamber with drift region
4.4 Anode charge waveforms
  4.4.1 Coaxial region approximation
  4.4.2 General case
  4.4.3 Induced charge on isolated anode wire
4.5 Cathode charge waveforms
  4.5.1 Continuous cathodes
  4.5.2 Wire cathodes
4.6 Approximation to microstrip avalanche chamber
4.7 Alternative approach
  4.7.1 Anode charge in standard geometry
  4.7.2 Cathode charge in standard geometry
  4.7.3 Chamber with drift region
  References

Chap.5 Multiwire geometry III
Cathode charge distributions
5.1 Exact distribution. Wire cathode
5.2 Exact distribution. Continuous cathode
  5.2.1 Distribution ρ_2
  5.2.2 Distribution ρ_1
5.3 Approximate distributions
  5.3.1 Distribution ρ_2
  5.3.2 Distribution ρ_1
5.4 Limiting cases approximate distributions
  5.4.1 Parallel plate geometry
  5.4.2 Pill-box geometry
5.5 Single parameter empirical formula
  References

Chap.6 Parallel plate geometry
Anode and cathode charge distributions
6.1 Introduction
6.2 Theory
  6.2.1 Basic formulae

- 6.2.2 Induced charge distributions
- 6.2.3 Collected charge distributions
- 6.2.4 Net charge distributions
- 6.3 Example distributions
- 6.4 Discussion
- References

Chap.7 Coaxial geometry II
Cathode charge distributions

- 7.1 Introduction
- 7.2 Basic theory
- 7.3 Azimuthal distribution of cathode charge
  - 7.3.1 Approximate formula
  - 7.3.2 Exact formula
- 7.4 Axial and azimuthal distribution of cathode charge
- 7.5 Current waveforms from radial streamers
  - 7.5.1 Introduction
  - 7.5.2 Anode current waveform
  - 7.5.3 Cathode sector current waveform
- References

Appendices

1. Weber approximation for MWPC potential
2. Derivation of single wire formula
3. Derivation of single strip formula
4. Evaluation of exponential integral
5. Evaluation of $H_0(\omega)$ and $H(\omega)$
6. Comments on gas gain formulae
7. Prompt electron signal in wire counters

Chapter 1.
BASIC THEORY AND DEFINITIONS

1.1 Methods of calculating induced charge

There are essentially two different approaches to the calculation of induced charge. The first, using the reciprocity theorem, is by far the most useful and will be employed in most of the applications described below. The second method, the evaluation of the surface field, has to be employed in special circumstances.

(i) The reciprocity method

Consider the system of conductors shown in Fig. 1.1. The relationship between the charges q_i and the potential V_i may be expressed in terms of geometrical configuration coefficients c_{ij} [1,2]. Thus,

$$q_i = \sum_{j=1}^{3} c_{ij} V_j$$

Suppose we wish to calculate the charge q_1 induced on conductor 1 by charge q_2 on conductor 2, all conductors other than 2 being grounded. Then

$$q_1 = c_{12} V_2 \qquad \text{and} \qquad q_2 = c_{22} V_2$$

Thus

$$q_1 = q_2 \ c_{12}/c_{22}$$

To calculate the ratio c_{12}/c_{22} consider now that conductor 1 is raised to unit potential, conductor 2 is insulated and uncharged and conductor 3 is grounded. Let P be the potential to which conductor 2 rises. Then

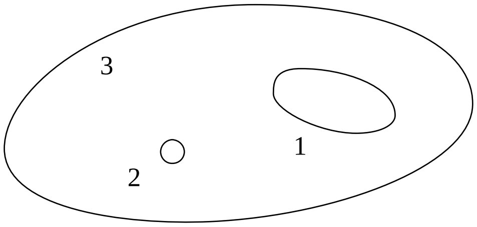

Figure 1.1

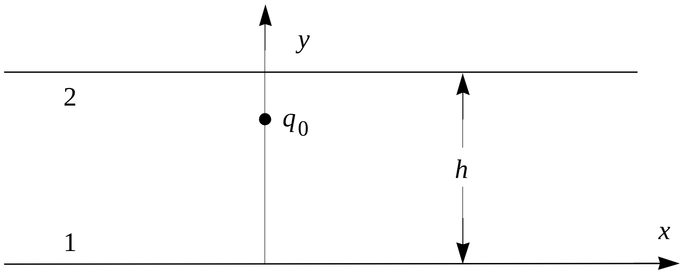

Figure 1.2

$$0 = c_{12} + c_{22}\ P \qquad \text{or} \qquad P = -c_{21}/c_{22}$$

But it is a property of the configuration coefficients that $c_{ij} = c_{ji}$ (Green's reciprocal theorem). Thus

$$q_1 = -Pq_2$$

The conductor 2 may be considered to be physically very small. That is we may regard a positive ion of charge q_2 mathematically as conductor 2.

Thus, to summarise, the charge q_i induced on the surface of a particular conductor by a point charge q_0 at (x, y, z) is equal to $-q_0P$, where P is the potential at (x, y, z) when that conductor is at unit potential all other conductors being grounded.

$$q_i = -q_0P \tag{1.1}$$

To illustrate the great power of this simple theorem consider the infinite parallel plate system of Fig. 1.2. If plate 1 is raised to unit potential with plate 2 grounded then the potential at distance y is simply

$$P(y) = (h - y)/h$$

Thus, by Eqn. 1.1 the charge induced on plate 1 by a point charge q_0 at y is

$$q_i = -q_0(1 - y/h) \tag{1.2}$$

This would otherwise be a quite lengthy calculation. However note that this particular application cannot yield the distribution of induced charge. The surface field method would have to be used, and this would involve summation of the field due to an infinite series of image charges. (See however Chapter 6.)

(ii) The surface field method

If the field E_n at the surface of a conductor can be evaluated, by any of the standard electrostatic methods, then the induced charge density is $\epsilon_0 E_n$, where ϵ_0 is the electrical space constant. This method has been employed below to calculate the induced charge distribution in a coaxial chamber (Chapter 7).

1.2 Ion trajectories

In order to investigate the development with time of the induced charge q_i, it is necessary to follow the trajectory $x(t)$, $y(t)$ of the inducing charge q_0. This latter is generally a separate calculation and should not be confused with the former. The induced charge on a particular electrode, N say, is $-q_0\, P_N(x,y)$ where $P_N(x,y)$ is the potential at (x,y) due to unit potential on electrode N all other electrodes being grounded. The trajectory $x(t), y(t)$, however, is formed from the derivatives of the potential $P(x,y)$, where $P(x,y)$ is the potential at (x,y) due to the operating potentials on all chamber electrodes. $P_N(x,y)$ and $P(x,y)$ may represent quite different calculations.

The positive ion mobility μ may usually be regarded as constant and the velocity of the ion is given by

$$\mathbf{v} = \mu \mathbf{E} \tag{1.3}$$

where $\mathbf{E}$ is the electric field due to the chamber operating voltages. Methods of calculating ion trajectories using this formula are given in detail below (Section 3.2)

It may sometimes be more useful to calculate directly the electrode induced current $i_i(x,y)$ rather than induced charge $q_i(x,y)$. This calculation can be represented, formally, as follows. Let the induced charge on electrode N be $-q_0\, P_N(x,y)$. Then the induced current is given by

$$i_i = -q_0 \frac{dP_N}{dt} = -q_0 \frac{dP_N}{d\ell} v$$

where $d\ell$ represents an increment of path in the direction of ion motion, that is in the direction of the applied field $\mathbf{E}$. Thus

$$i_i = -q_0 \mu (\mathbf{E_N} \cdot \mathbf{E}) \tag{1.3}$$

where $\mathbf{E_N} = -$ grad P_N. Of course calculation of i_i as a function of time also required knowledge of the ion trajectory $x(t), y(t)$.

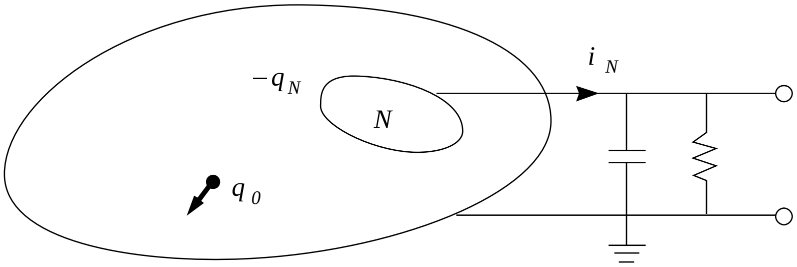

Figure 1.3

1.3 Induced charge and signal charge

Let the charge induced on the surface of electrode N by point charge q_0 be $-q_N$, see Fig. 1.3. From Eqn. (1.1) $-q_N = -q_0 P_N$. Then the signal charge, that is the observable charge, is $-(-q_N) = q_N$.

Thus signal charge q_N and signal current i_N are given by, respectively,

$$q_N = q_0\, P_N(x, y) \tag{1.4a}$$

$$i_N = q_0 \frac{dP_N(x, y)}{dt} \tag{1.4b}$$

The resulting signal waveforms depend also on the signal processing of i_N (see Section 1.5 below).

Of course in proportional counters and chambers, one electrode, the anode, receives a negative (electron) charge. This is usually assumed to occur as a delta function of time (but for exception see comment in Section 1.5). If the ion charge is q_0 then this electron charge must have been $-q_0$. Thus if electrode A is the anode of the system, the net anode signal charge is

$$q_a = -q_0 + q_A = -q_0(1 - P_A) \tag{1.5}$$

If there are only two electrodes, with electrode C enclosing electrode A (e.g. a coaxial counter) then

$$\begin{aligned} &q_a = -q_0(1 - P_A) \\ &q_c = q_0 - q_A = q_0(1 - P_A) = -q_a \end{aligned}$$

1.4 Nomenclature

An attempt will be made to employ a consistent nomenclature, that employed above, throughout these notes. Thus the inducing point charge, positive, will be denoted by q_0. The induced charge on the surface of electrode N will be $-q_N$ so that the signal (observable) charge is then q_N. The net charge on electrode N, will be denoted by use of lower case subscript, as in the previous section. If the signal charge and net charge are the same (i.e. no collected charge) then lower case subscript will generally be used. The potential due to unit potential on electrode N, all other electrodes being grounded, will be $P_N(x, y)$.

If these conventions are not able to be followed then special comment will be made.

1.5 Signal processing

It is not the intention to discuss signal processing in detail in these notes but, for completeness, some very brief observations may be made in this introductory section. (see also Section 2.4).

If $q_n(t)$ or $i_n(t)$ is obtained (generally numerically) then the processing system output may be obtained by convolution with the appropriate system impulse response. In every case of practical interest this convolution has to be performed numerically but, using library integration routines now available, completely adequate accuracy can be readily achieved.

If the primary excitation is not itself a delta function, for example due to diffusion before the avalanche or due to finite photoelectron range, then the output waveform must be further convoluted with the primary waveform to obtain a final result. This last procedure is required in certain circumstances (for example if accurate knowledge of the initial slope of the output waveform is of importance, as in pulse shape discrimination).

1.6 The avalanche charge q_0

The avalanche is assumed to produce an electron charge $-q_0$ and therefore also a positive ion charge q_0. In all wire chambers it will be assumed that the final stage of this avalanche occurs so close to the anode wire surface that the electron component of the anode signal is negligible. (See Appendix 7 for quantitative justification.) This cannot be assumed in a parallel plate chamber. In both wire chambers and parallel plate chambers the avalanche electron collection time is assumed to be negligible.

Determination of the magnitude of q_0 in terms of the anode potential and gas physics, that is the determination of gas gain, is a complicated problem that would require a further monograph to unravel. A few brief comments to indicate how the magnitude of q_0 might be estimated are given in Appendix 6.

1.7 Geometry limitations

Readers of this monograph are reminded that most of the problems studied concern systems in which the electrode geometry can be regarded as remaining constant with respect to one coordinate (the z-axis). Thus chamber wires are normal to the $x - y$ plane and mathematical infinitely long. Under these conditions the potential distribution due to the electrode potentials becomes a function of x, y only, and hence several powerful and well-established methods (the use of complex variables) may be used to obtain suitable solutions.

References

1. J.C. Maxwell, A treatise on electricity and magnetism (3rd Ed.), Oxford University Press, London, 1892.
2. W.R. Smythe, Static and dynamic electricity, McGraw-Hill, New York, 1950.

Chapter 2.

COAXIAL GEOMETRY I

The simple results derived below are long-established and well-known. However it will be very convenient for later work to have collected here some important, basic formulae.

2.1 Formulae for field, potential and capacitance [1]

Consider a coaxial chamber, with anode radius r_a and cathode radius r_c, length very large compared with r_c, anode at potential V_a and with grounded cathode, Fig. 2.1. Then the field at radius r is given by

$$E = 2CV_a/r \tag{2.1}$$

where

$$C = 1/\ln(r_c/r_a)^2 \tag{2.2}$$

The capacitance per unit length of anode is

$$C_1 = 4\pi\epsilon_0 C \tag{2.3}$$

where ϵ_0 is the electrical space constant.*
The potential at radius r is given by

$$P = V_a[1 - C\ln(r/r_a)^2] \tag{2.4}$$

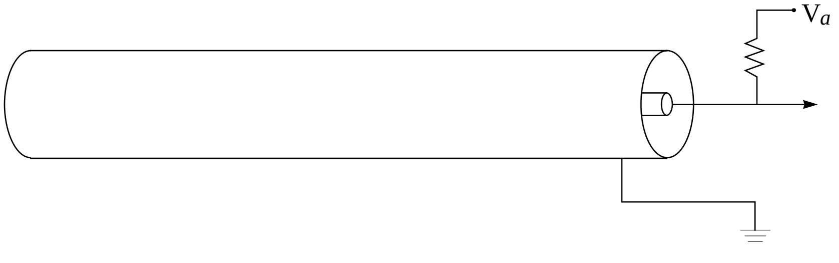

Figure 2.1

---

* $4\pi\epsilon_0 = 0.1113$ pF/mm

2.2 Anode induced and net charges

Unit potential on the anode, the cathode being grounded, produces a potential distribution, from Eqn. 2.4,

$$P_A = 1 - C\ln(r/r_a)^2$$

Thus if the avalanche results in a positive point charge q_0 at radius r then, from Eqn. 1.1, the anode induced charge is

$$-q_A = -q_0[1 - C\ln(r/r_a)^2] \tag{2.5}$$

and therefore, from Eqn. 1.5, the anode net charge is

$$q_a = -q_0 C\ln(r/r_a)^2 \tag{2.6}$$

Clearly the cathode signal, and net, charge is $q_c = -q_a$.
That is

$$q_c = q_0 C\ln(r/r_a)^2 \tag{2.7}$$

2.3 Time development of anode charge

The ion velocity is radial and of magnitude given by, Eqns. 1.2 and 2.1,

$$\frac{dr}{dt} = \mu E = \frac{2\mu C V_a}{r} \tag{2.8}$$

Thus

$$\int_{r_a}^{r} r\,dr = 2\mu C V_a t$$

or

$$(r/r_a)^2 = 1 + 4\mu C V_a t/r_a^2 \tag{2.9}$$

It is convenient to define a characteristic counter time t_0.

$$t_0 = r_a^2/4\mu C V_a \tag{2.10}$$

Thus

$$(r/r_a)^2 = 1 + t/t_0 \tag{2.11}$$

and

$$q_a(t) = -q_0 C\ln(1 + t/t_0) \tag{2.12}$$

This functional dependence on time t was obtained by Wilkinson [2]. Typical values for C and t_0 for a small coaxial counter are 0.07 and 0.5 nanoseconds respectively.

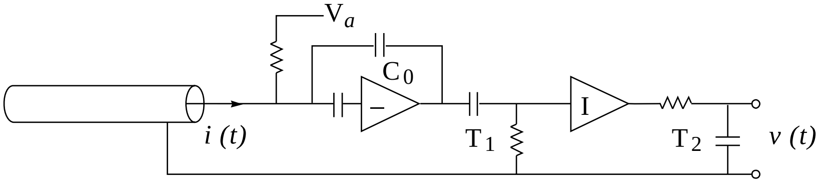

Figure 2.2

Despite the very fast rise time of the charge pulse, as shown by Eqn. 2.12, the ions are not collected at the cathode until a time t_c many orders of magnitude greater than t_0. It follows from Eqn. 2.12 that

$$t_c/t_0 = (r_c/r_a)^2 - 1$$

The collection time t_c may be several tens to several hundred of microseconds.

At very high count rates a large counter may contain an appreciable charge of drifting positive ions. The effects of this positive ion space charge are described briefly in Section 3.6.

2.4 Signal processing

As a brief illustration consider the standard system shown in Fig. 2.2. A charge-sensitive amplifier is followed by an amplifier with differentiating time constant T_1 and integrating time constant T_2. (In practice T_1, T_2 are of the order 0.2 to 2μs.) The transfer impedance for the system is $H(s)$ given by

$$H(s) = -\frac{1}{sC_0}\frac{s}{s+1/T_1}\frac{1/T_2}{s+1/T_2}$$

and hence the impulse response is

$$h(t) = -\frac{1}{C_0}\frac{T_1}{T_1-T_2}\left(e^{-t/T_1} - e^{-t/T_2}\right)$$

Then it is easily shown that for counter current, from Eqn. 2.12,

$$i(t) = -q_0 C/(t+t_0) \tag{2.13}$$

the output voltage is given by

$$v(t) = q_0\frac{C}{C_0}\frac{T_1}{T_1-T_2}\{f(t,t_0,T_1) - f(t,t_0,T_2)\}$$

where

$$f(t, t_0, T) = e^{-(t+t_0)/T} \int_{t_0/T}^{(t+t_0)/T} \frac{e^z}{z}\, dz$$

Thus even in this very simple case a final analytical solution is not possible. However the exponential integral can now be evaluated numerically to any required degree of accuracy (with sufficient care; see Appendix 4). Special treatment is required for $T_1 = T_2$, but presents no difficulties.*

This method can be readily adapted to treat all standard signal processing methods.

References

1. W.R. Smythe, Static and dynamic electricity, McGraw Hill, New York 1950.
2. D.H. Wilkinson, Ionisation chambers and counters, Cambridge University Press, Cambridge, 1950.

---

* If $T_1 = T_2 = T$, say, then

$$\nu(t) = q_0 \frac{C}{C_0} \left\{ \frac{t+t_0}{T} f(t, t_0, T) + e^{-t/T} - 1 \right\}$$

Chapter 3.
MULTIWIRE GEOMETRY I.
Weber approximation

3.1 Introduction

The multiwire proportional chamber, developed originally by Charpak and his colleagues at CERN [1], has been applied over a remarkably wide range of investigations. These have included important, central experiments in high-energy physics, X-ray crystalography and astrophysics. Further applications are still being developed.

The geometry of a conventional, symmetric multiwire chamber is shown schematically in Fig. 3.1. As in all the multiwire geometries studied in this monograph it is assumed that $r_a \ll s$, and that the electrodes extend mathematically to infinity normal to the $x - y$ plane.

If it can be further assumed that the anode, cathode spacing h is such that $\cosh 2\pi h/s \gg 1$, where s is the (constant) anode wire pitch, then the Weber approximation [2] for potential distribution may be employed (see Appendix 1). This leads to considerable simplifications in the formal analysis. In practice this approximation is generally useful for $h \gtrsim 2s$.

This chapter will develop formulae assuming that the Weber approximation is valid. There are however many important problems which cannot be treated in this formulation, quite apart form the validity of $\cosh 2\pi h/s \gg 1$. These include the calculation of cathode charge distribution, the analysis of chambers with wire cathodes and drift regions, the calculation of induced charge on isolated wires or particular groups of wires, etc. These and other problems will be addressed in Chapter 4, where a general method of approach will be described.

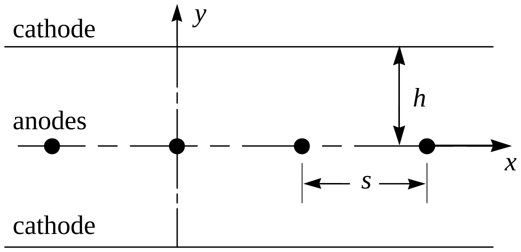

Figure 3.1

3.2 Potential, capacitance and field formulae

3.2.1 Potential distribution. Anode at unit potential

It is shown in Appendix 1 that the potential function $P_W(x, y)$ due to the anode in Fig. 3.1 being at unit potential, the cathodes being grounded, is

$$P_W(x, y) = 1 - C \ln \frac{2(\cosh 2\pi y/s - \cos 2\pi x/s)}{(2\pi r_a/s)^2} \tag{3.1}$$

where

$$C = 1/\ln(r_c/r_a)^2 \tag{3.2a}$$

and

$$r_c \equiv (s/2\pi)e^{\pi h/s} \tag{3.2b}$$

It is instructive to note the form of Eqn. 3.1 in the two limiting regions.

i) $x, y \ll s$.

By expansion of the curly bracket in Eqn. 3.1, and by placing $(x^2 + y^2)^{1/2} = r$, it is found that

$$P_W(r) = 1 - C \ln(r/r_a)^2 \tag{3.3}$$

Thus, as expected, close to an anode wire, the potential has coaxial form.

ii) $\cosh 2\pi y/s \gg 1$ then

$$P_W(y) = \frac{2\pi C}{s}(h - |y|) \tag{3.4}$$

In this case, in the main body of the chamber, the potential falls uniformly with $|y|$. The field in this region, per unit anode potential, is simply $\pm 2\pi C/s$.

3.2.2 Potential distribution. Cathode at unit potential

If the upper cathode, in Fig. 3.1, is at unit potential and the anode wires and lower cathode are grounded then the analysis of Appendix 1 shows that the potential function $P_C(x, y)$ is given by

$$P_C(x, y) = \frac{y}{2h} + \frac{C}{2} \ln \frac{2(\cosh 2\pi y/s - \cos 2\pi x/s)}{(2\pi r_a/s)^2} \tag{3.5}$$

It is again interesting to note the form of P_C in the limiting regions.

i) $x, y \ll s$

$$P_C = \frac{y}{2h} + \frac{c}{2} \ln \left(\frac{r}{r_a} \right)^2 \tag{3.6}$$

ii) $\cosh 2\pi y/s \gg 1$

$$P_C = \frac{1}{2}\left(1 + \frac{y}{h}\right) - \frac{\pi C h}{s}\left(1 - \frac{|y|}{h}\right) \tag{3.7}$$

3.2.3 Capacitance per unit length

It was shown in Section 3.2.1 that the potential close to an anode wire has coaxial form, Eqn. 3.3. The capacitance per unit length of each anode wire is therefore C_1 given by

$$C_1 = 4\pi\epsilon_0 C \tag{3.8}$$

where C has been defined in Eqn. 3.2.

Further formulae for C will be developed, for $h \ll s$ (Section 4.2), and for the general case (Section 4.3.2).

3.2.4 Field formulae

These are obtained at once by partial differentiation of Eqn. 3.1. Thus, for anode potential V_a, the cathodes being grounded

$$E_x = -V_a \frac{\partial P_W}{\partial x} = 2CV_a \frac{\pi}{s} \frac{\sin 2\pi x/s}{\cosh 2\pi y/s - \cos 2\pi x/s} \tag{3.9a}$$

$$E_y = -V_a \frac{\partial P_W}{\partial y} = 2CV_a \frac{\pi}{s} \frac{\sinh 2\pi y/s}{\cosh 2\pi y/s - \cos 2\pi x/s} \tag{3.9b}$$

The resultant field $E = (E_x^2 + E_y^2)^{\frac{1}{2}}$ is given by

$$E = 2CV_a \frac{\pi}{s} \left\{ \frac{\cosh 2\pi y/s + \cos 2\pi x/s}{\cosh 2\pi y/s - \cos 2\pi x/s} \right\}^{1/2} \tag{3.10}$$

The two limiting regions have very simple forms

i) $x, y \ll s$ $\quad E = 2CV_a/r$ $\quad$ coaxial field

ii) $\cosh 2\pi y/s \gg 1$ $\quad E_x = 0, E_y = \pm 2\pi CV_a/s$ $\quad$ uniform field

See, however, Section 4.3 for a further discussion of the approximation near region i).

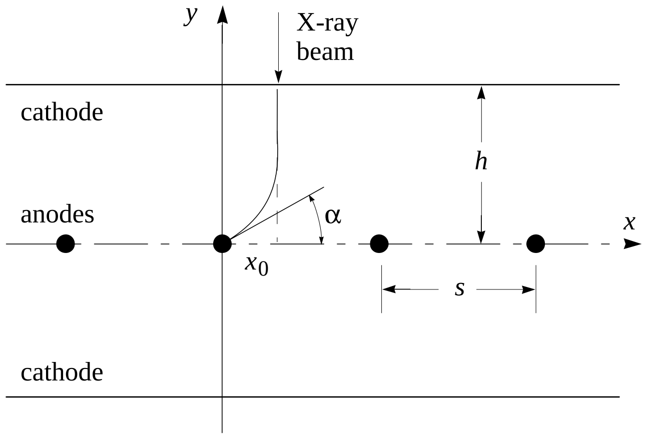

Figure 3.2

3.3 Field lines and ion trajectories

3.3.1 Field line formulae

From the analysis given in Appendix 1 it is seen that the field lines, from the central anode wire to the cathode, are described by the expression

$$\tanh \pi y/s = \tan \pi x/s \, \tan \alpha \tag{3.11}$$

where α is the angle, measured from the x-axis, at which a field line leaves the anode wire surface, Fig. 3.2.

If $\cosh 2\pi y/s \gg 1$ then there is a simple linear relationship between the coordinate in the uniform field region, x_0, and α. From Eqn. 3.11

$$\alpha = \frac{\pi}{2}\left(1 - \frac{2x_0}{s}\right) \tag{3.12}$$

This equation is relevant when considering the effects of avalanche angular localization [3].

If for some reason the upper cathode is not grounded but held at a potential V_R relative to the anode potential then the analysis of Appendix 1 shows that the field line equation becomes modified to

$$\tanh \pi y/s = \tan \pi x/s \cdot \tan\left\{\alpha - \frac{xV_R}{4hC(1 - V_R/2)}\right\} \tag{3.13}$$

3.3.2 Ion trajectories

In order to calculate ion trajectories as a function of time it is necessary to determine the velocity components through the equations

$$\frac{\partial x}{\partial t} = -\mu V_a \frac{\partial P_W}{\partial x} \tag{3.14a}$$

$$\frac{\partial y}{\partial t} = -\mu V_a \frac{\partial P_W}{\partial y} \tag{3.14b}$$

In numerical calculations it is very convenient to employ normalised quantities. Thus Eqn. 3.14 above can be written

$$\frac{\partial x'}{\partial t'} = -\frac{\partial P_W}{\partial x'} \tag{3.15a}$$

$$\frac{\partial y'}{\partial t'} = -\frac{\partial P_W}{\partial y'} \tag{3.15b}$$

where $x' = x/s$, $y' = y/s$ and $t' = t/T_0$ where

$$T_0 = s^2/\mu V_a \tag{3.16}$$

Linear dimensions are normalized to the anode wire pitch s, and times are normalized to the quantity T_0. In a typical MWPC T_0 has the value of a few microseconds.

The numerical method employed by the writer to calculate ion trajectories may be described very briefly as follows. A small path increment is chosen, of the order 1μm but actual value depending upon the particular situation. Velocity components, and resultant velocity are calculated according to Eqn. 3.15. From the resultant velocity components the two spatial components of the path increment are obtained. Thus a new point on the trajectory can be constructed. This is a very simple procedure where accuracy clearly depends upon the initial choice of the path increment. For normal situations adequate accuracy is easily and quickly obtained.

3.4 Ion collection times

3.4.1 Average ion collection time

Although not dependent upon the Weber approximation it is convenient at this point to present a very general argument by which the average ion collection time can be determined [4].

Consider a tube of electrical flux $d\phi$, of unit depth along the z-axis, and a position where the cross-sectional area is say dA, Fig. 3.3. Let the

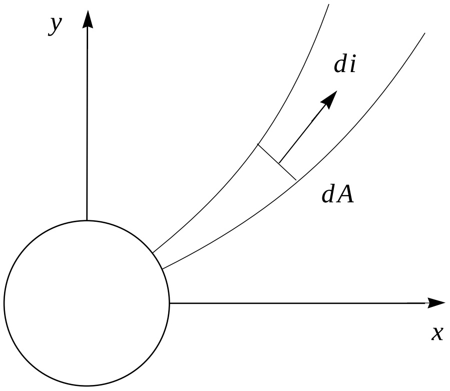

Figure 3.3

anode wires of the chamber each be counting at the rate n_1 per unit length, generating for each event a charge q_0. It will be assumed that the avalanche events are uniformly distributed round each wire. Thus the ion current into the tube of flux is

$$di = n_1 q_0 d\alpha / 2\pi \tag{3.17}$$

where $d\alpha$ is the angular width of the tube at the surface of the wire. This current remains constant along the tube.

Let the ion charge density at the cross-section dA be ρ. Then the current through dA is $\mu E \rho dA = \mu \rho d\phi / \epsilon_0$. However the flux $d\phi$ is given, in terms of anode voltage V_a, by

$$d\phi = C_1 V_a d\alpha / 2\pi$$

where C_1 is the capacitance per unit length of anode wire. Thus

$$di = 2\mu C V_a \rho d\alpha \tag{3.18}$$

where C_1 has been replaced by $4\pi\epsilon_0 C$, Eqn. 3.8. Thus equating the two expressions for the current di, Eqns. 3.17 and 3.18, an expression for ρ is obtained.

$$\rho = \frac{n_1 q_0}{4\pi \mu C V_a} \tag{3.19}$$

Thus, remarkably, the average ion charge density ρ is independent of position. Further, the derivation of Eqn. 3.19 was not specific to a particular geometry; the result applies to both coaxial and multiwire chambers [4].

Considering now the multiwire geometry of Figs 3.1 and 3.2 the volume per unit length of each anode wire cell is $2hs$. Thus the average stored charge per unit length of cell is simply $2hs\rho$. But the average current per unit length of wire is $n_1 q_0$. Hence the average collection time for ions is $t_{av} = 2hs\rho/n_1 q_0$, or,

$$t_{av} = \frac{hs}{2\pi\mu C V_a} = T_0 \frac{h/s}{2\pi C} \tag{3.20}$$

where $T_0 = s^2/\mu V_a$.

This is a useful, general result and important in considering the reduction in pulse height in MWPCs due to high count rates. (See Section 3.6)

In a typical small chamber t_{av} is of the order 50μs.

3.4.2 Minimum ion collection time

In the present approximation, $\cosh 2\pi h/s \gg 1$, a simple analytical expression can be obtained for the minimum ion collection time, that is when $\alpha = \pi/2$, Fig 3.2. In this case, since $x = 0$ in Eqn. 3.9,

$$E_y = 2CV_a \frac{\pi}{s} \coth \frac{\pi y}{s}$$

Then

$$t_{\min} = \int_{r_a}^{h} \frac{dy}{\mu E_y} = \frac{s}{2\pi\mu C V_a} \int_{r_a}^{h} \tanh \frac{\pi y}{s}\, dy$$

$$= \frac{(s/\pi)^2}{2\mu C V_a} \ln \frac{\cosh \pi h/s}{\cosh \pi r_a/s}$$

Since $\cosh \pi h/s \gg 1$ and $r_a \ll s$ this last result may be written

$$t_{\min} = T_0 \frac{h/s}{2\pi C} \left(1 - \frac{\ln 2}{\pi h/s}\right) \tag{3.21}$$

Thus, for example, for $h = 2s$ the minimum collection time is about 11% less than the average collection time t_{av}.

3.5 Anode and cathode charge waveforms

3.5.1 Coaxial region approximation

If the ions can be considered as moving in the essentially coaxial region of the avalanche anode wire then the anode waveform can be written down at once, from Eqns. 2.12 and 3.2. That is

$$q_a(t) = -q_0 C \ln(1 + t/t_0)$$

where $C = 1/\ln(r_c/r_a)^2$, $r_c = (s/2\pi)e^{\pi h/s}$ and $t_0 = r_a^2/4\mu C V_a$. For typical MWPC geometry this waveform should be a useful approximation for t below about one microsecond.

3.5.2 General case

If signal processing time constants are long enough that the ions have moved from the coaxial region then, generally, the anode and cathode waveforms must be constructed numerically. That is, from Eqns. 1.5 and 1.4a,

$$q_a = -q_0[1 - P_W(x, y)] \tag{3.22}$$

$$q_c = q_0 P_C(x, y) \tag{3.23}$$

where $P_W(x, y)$ and $P_C(x, y)$ have been given in Equs 3.1 and 3.5 respectively. The trajectory $x(t), y(t)$ can be constructed using the formulae of Section 3.3.

Because of the finite differentiating time constant that must be employed in any signal processing system, the variation of $P_W(x, y)$ with initial angle α (Section 3.3) results in a small but significant dependence of output pulse height on α. Quantitative evaluation of this effect has been given in ref. [4].

In a practical situation the electron avalanche must exhibit a finite angular spread about a centroid position α. In order then to simulate the anode waveform a weighted 'fan' of ion trajectories must be employed in the model [5,6]. This procedure becomes especially important when considering the two cathode waveforms.

It is clear already from Eqn. 3.6 that the two induced cathode charges will be considerably more sensitive to the initial ion angle α than the anode charge. Quantitative evaluation of $q_c(t)$ from Eqn. 3.23 has indeed allowed a measure to be made of the avalanche angular spread [5]. Examination of the cathode pulse heights, or rise-times, allows a very clear distinction to be made between 'near-side' and 'far-side' events.

3.5.3 Dependence of gas gain on α

A second effect also results in a dependence of pulse height on ion initial angle α. Because of the finite departure from a strictly coaxial field, even close to the anode wire where the avalanche forms, the gas gain itself is a function of α. This effect may be evaluated quantitatively as follows.

The expression for field, Eqn. 3.10, may be expanded in the region $x, y \ll s$, retaining second order terms as well as first order terms. The result is

$$E = \frac{2CV_a}{r}\left\{1 - \frac{1}{3}\left(\frac{\pi r}{s}\right)^2 \cos 2\alpha\right\} \tag{3.24}$$

where $\tan\alpha = y/x$.

In order to obtain a closed formula for the gas gain, let us assume a simple linear dependence of the Townsend coeficient α_T on field. That is, $\alpha_T = B(E - E_0)$ where B and E_0 are constants. (Typically $B \sim 30\text{kV}^{-1}$ and $E_0 \sim 20\text{kV/cm}$.) The gas gain M may be calculated from the relationship

$$\ln M = \int_{r_a}^{r_0} \alpha_T dr = \int_{r_a}^{r_0} B(E - E_0)dr$$

where $r_0 = 2CV_a/E_0$. The gas gain M_0 at $\alpha = \pi/4$ is readily shown to be given by

$$\ln M_0 = 2CV_a B\{\ln(r_0/r_a) - 1 + r_a/r_0\} \tag{3.25}$$

After some manipulation, and assuming that the fractional change $\Delta M/M_0$ is small compared with unity, it is found that

$$\Delta M/M_0 \simeq -\frac{2B}{3}\left(\frac{\pi}{E_0}\right)^2 \frac{(CV_a)^3}{s^2} \cos 2\alpha \tag{3.26}$$

This is a simpler formula than originally derived [4], but the dependence on V_a^3/s^2 remains as before.

In reality the variation in gain with α would be rather smaller than expressed by Eqn. 3.26 because of the finite angular spread of the avalanche. This smoothing effect may be evaluated in the following manner. Assume that the avalanche angular distribution can be described by a gaussian with rms spread σ and total number of primaries n_0. That is

$$n(\alpha) = \frac{n_0}{\sqrt{2\pi\sigma^2}} e^{-(\alpha-\alpha_0)^2/2\sigma^2} \tag{3.27}$$

and the average gas gain at centroid angle α_0 is

$$M_{av} = \frac{1}{n_0}\int_{-\infty}^{\infty} nM d\alpha \tag{3.28}$$

Eqn. 3.26 may be conveniently expressed

$$M = M_0 \left(1 - k \cos 2\alpha\right) \text{ where } k = \frac{2B}{3}\left(\frac{\pi}{E_0}\right)^2 \frac{\left(CV_a\right)^3}{s^2}$$

Then the result of the integration, Eqn. 3.28, may be written

$$(M_{av} - M_0)/M_0 = \Delta M_{av}/M_0 = -k \cos 2\alpha_0 e^{-2\sigma^2} \tag{3.29}$$

Thus the spreading of the avalanche, due to diffusion, photoelectron range and intrinsic
avalanche processes, introduces a strong modifying factor $e^{-2\sigma^2}$. The effect of a non-coaxial field is therefore quite rapidly smoothed out. For example, if $\sigma = \pi/4$ then this modifying factor is ~ 0.3.

Comparison between experimental measurement and theoretical prediction of the dependence of gas gain on α_0 has been reported in ref. [7]. In that same report it is also demonstrated that this dependence can be effectively suppressed by suitable geometry of the upper wire cathode.

3.6 Dependence of gas gain on count rate

It is convenient to end this chapter with some brief, but quantitative, comments on the dependence of gas gain on count rate. Because of the comparatively long ion collection time (tens to hundreds of microseconds), a significant positive space charge becomes stored in a chamber when operated at high count rates. This space charge reduces the field near the anode wire surface and hence reduces the gas gain. This effect can be described quantatively as follows.

Suppose, for the present argument, that a large area of chamber is uniformly irradiated, and that each anode wire is counting at the rate n_1 per unit length. Then, as shown in Section 3.4.1, the average ion charge density in the chamber in constant, independent of position, and given by

$$\rho = \frac{n_1 q}{4\pi\mu C V_a} \tag{3.30}$$

Here q is the avalanche charge per count.

This positive ion space charge induces on the anode wire surfaces a negative charge such that the wire surface is an equipotential (a zero potential superimposed, of course, on the operating voltage V_a). Now provided the anode wire radius is small compared with the other chamber dimensions this induced charge can be considered to be uniform line charges coincident with the wire axes. Each line charge produces at the position of the anode wire surface a potential $-\delta V$ where $+\delta V$ is the potential which would be produced at that position in the absence of the anode wires by the space charge. The space charge field at the wire surfaces is therefore simply that that would be obtained by a change in operating voltage $-\delta V$. It simply remains to relate δV and ρ.

Straightforward application of Gauss's theorem shows that uniform charge density ρ in the chamber would produce, in the absence of anode wires, a potential distribution

$$P = \frac{\rho}{2\epsilon_0}(h^2 - y^2) \tag{3.31}$$

Thus in the plane $y = 0$

$$\delta V = \frac{\rho h^2}{2\epsilon_0} \tag{3.32}$$

or

$$\delta V = \frac{n_1 q h^2}{2\mu C_1 V_a} \tag{3.33}$$

where $C_1 = 4\pi\epsilon_0 C$ is the capacitance per unit length of wire, Section 3.2.3.

Now it is known experimentally that, for both coaxial and multiwire chambers, over a limited range of gain change (about two to one), $\ln M$ is a nearly linear function of V_a. That is, over the typical range observed for gain reduction due to space charge, the quantity $(1/M)dM/dV_a$ is essentially constant. Thus if q is the avalanche charge and q_0 the avalanche charge when the ion space charge is negligible,

$$\ln\frac{q}{q_0} = -\frac{1}{M}\frac{dM}{dV_a}\delta V \tag{3.34}$$

or

$$\ln\frac{q}{q_0} = -\frac{1}{M}\frac{dM}{dV_a}\frac{n_1 q h^2}{2\mu C_1 V_a} \tag{3.35}$$

It is instructive to write this last equation in the form

$$\frac{\ln(q/q_0)}{q/q_0} = -\frac{n_1 q_0}{I_m} \tag{3.36}$$

where

$$I_m = \left(\frac{R_m}{M}\frac{dM}{dV_a}\right)^{-1} \tag{3.37}$$

and

$$R_m = h^2/2\mu C_1 V_a \tag{3.38}$$

Thus the performance of a counter with respect to count rate may be conveniently described by a characteristic current density I_m (or a characteristic resistivity R_m). Typically $(1/M)dM/dV_a \approx 7 \times 10^{-3}\text{V}^{-1}$ and I_m is in the range 1–20nA/mm.

It is easily shown that for coaxial geometry, replacing R_m by R_c,

$$R_c = r_c^2/4\mu C_1 V_a \tag{3.39}$$

The above analysis has considered only the case of uniform irradiation over an unrestricted area. General treatments have been given, for coaxial counters by Sipila et al. [8], and for multiwire chambers and coaxial counters by Mathieson [9].

It was an interesting scientific accident that the detailed experiment measurements on coaxial counters of Sipila & Vanha-Honko [10] appeared to be in a good agreement with a theoretical formula developed by Hendricks [11] which, unfortunately, was in error by a factor π. Sipila et al. [8], who then made a more detailed study of the problem, were able to explain their apparent agreement in terms of the finite irradiation length used in their experiments.

Experimental verification of the theory developed for MWPCs [9] may be found in ref. [12].

References

1. G. Charpak, R. Bouclier, T. Bressani, J. Favier & Č. Zupančič, Nucl. Instr. & Meth. 62 (1968) 262; 65 (1968) 217.
   G. Charpak, D. Rahm & H. Steiner, Nucl. Instr. & Meth. 80 (1970) 13.
   G. Charpak, Nucl. Instr. & Meth. 156 (1978) 1.
2. E. Weber, Electromagnetic Fields, Wiley, New York, 1950.
3. A.H. Walenta, J. Heintze & B. Schürlein, Nucl. Instr. & Meth. 92 (1971) 373.
   G. Charpak, Nature 270 (1977) 479.
   J. Fischer, H. Okuno & A.H. Walenta, IEEE Trans. Nucl. Sci. NS-25 (1978) 794.
   E. Mathieson, T.J. Harris & G.C. Smith, Nature 272 (1978) 709.
   T.J. Harris & E. Mathieson, Nucl. Instr. & Meth. 154 (1978) 183.
4. E. Mathieson & T.J. Harris, Nucl. Instr. & Meth. 157 (1978) 563.
5. E. Mathieson & T.J. Harris, Nucl. Instr. & Meth. 159 (1979) 483.
6. J.S. Gordon & E. Mathieson, Nucl. Instr. & Meth. 227 (1984) 267.

7. E. Mathieson & G.C. Smith, IEEE Trans. Nucl. Sci. NS-37 (1990) 187.
8. H. Sipila, V. Vanha-Honko & J. Bergquist, Nucl. Instr. & Meth. 176 (1980) 381.
9. E. Mathieson, Nucl. Instr. & Meth. A249 (1986) 413.
10. H. Sipila & V. Vanha-Honko, Nucl. Instr. & Meth. 153 (1978) 461.
11. R.W. Hendricks, Rev. Sci. Instr. 40 (1969) 1216.
12. G.C. Smith & E. Mathieson, IEEE Trans. Nucl. Sci. NS-34 (1987) 410.

Chapter 4.

MULTIWIRE GEOMETRY II.
General treatment

4.1 Introduction

There are several important practical situations in which the method of Chapter 3 cannot be employed, or simply in which the basic condition for the validity of the Weber approximation is not met. The present chapter describes a general method for calculating potential, fields and induced charges which has no restricting condition (other than $r_a \ll s$, and the assumption of uniform geometry in the z-direction), [1,2]. The chamber need not be symmetric with respect to anode, cathode spacings and it may contain a wire cathode and a drift region. The width of the anode plane can be finite if necessary. The anode, or cathode, wires can have non-uniform pitch, or non-uniform radii, although in practice these conditions are very seldom encountered (however, see Section 4.6). Except in Section 4.6 wire radii and wire pitch will be assumed to be constants in the following analyses.

Having calculated potentials and fields due to a specific electrode configuration, the general methods already described in previous chapters can be used to determine the induced charge on a particular electrode.

4.2 Potential and capacitance due to single wire

It is shown in Appendix 2 that the potential due to a line charge of linear density q at (x_0, y_0), parallel to infinite grounded cathodes normal to the x, y plane as shown in Fig. 4.1, is given by

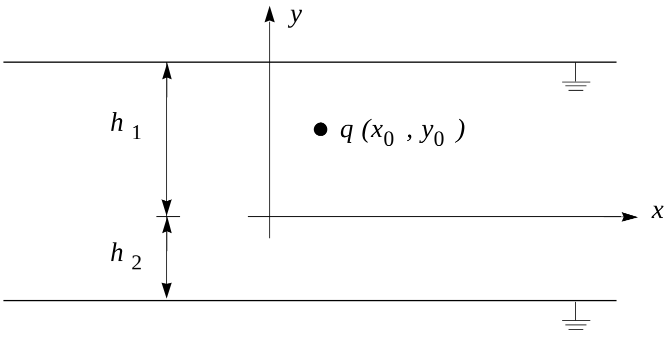

Figure 4.1

$$P(x, y, x_0, y_0) = -\frac{q}{2\pi\epsilon_0} L(x, y, x_0, y_0) \tag{4.1a}$$

where

$$L(x, y, x_o, y_0) = \ln \left\{ \frac{\cosh a(x - x_0) - \cos a(y - y_0)}{\cosh a(x - x_0) + \cos a(y + y_0 - d)} \right\}^{1/2} \tag{4.1.b}$$

and $a = \pi/2h, \quad h = (h_1 + h_2)/2, \quad d = h_1 - h_2.$

This basic formula may be adapted and modified for application to all MWPC field and potential calculations.

Before proceeding to study multiwire chambers it is instructive to consider a simple application. Assume that a wire of radius r_a small compared with h_1 and h_2, and at potential V_a, is situated at the coordinate origin. Eqn. 4.1 above, with $x_0 = y_0 = 0$, yields the potential function, but we need to evaluate the unknown q in terms of V_a (that is, we must find the capacitance per unit length C_1). Let $x \to 0$ and $y \to 0$ with $x^2 + y^2 = r^2$. Then

$$L(r) \to \ln \frac{ar/2}{\cos(ad/2)} \tag{4.2}$$

When $r = r_a$, that is at the wire surface, $P = V_a$. Thus

$$V_a = -\frac{q}{2\pi\epsilon_0} \ln \frac{ar_a/2}{\cos(ad/2)}$$

Hence

$$C_1 = \frac{4\pi\epsilon_0}{\ln \left[\dfrac{\cos(ad/2)}{ar_a/2} \right]^2}$$

It is convenient, as in Section 3.1, to write

$$C_1 = 4\pi\epsilon_0 C \tag{(3.8)}$$

and to define an effective cathode radius r_c such that

$$C = 1/\ln(r_c/r_a)^2$$

Thus

$$r_c = \frac{4h}{\pi} \cos\left(\frac{\pi d}{4h}\right)$$

If, as is usual, $h_1 = h_2 = h$ then $d = 0$ and

$$r_c = 4h/\pi \tag{4.3}$$

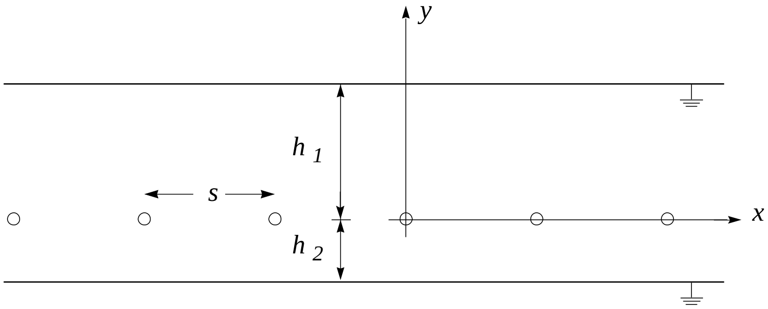

Figure 4.2

This value of r_c should be compared with the value given in Eqn. 3.2. The two equations 4.3 and 3.2 represent limiting values corresponding respectively to very large and very small anode wire pitch compared with anode, cathode spacing. Section 4.3.2 will establish a formula for the general case.

The potential distribution due to a wire, at the origin at potential V_a can now be written

$$P(x,y) = -2CV_a\,L(x,y) \tag{4.4a}$$

$$L(x,y) = \ln\left\{\frac{\cosh ax - \cos ay}{\cosh ax + \cos a(y-d)}\right\}^{1/2} \tag{4.4b}$$

The basic principles, described in Chapter 1 and in Sections 3.5 and 3.2, may now be applied to calculate the anode charge waveform $q_a(t)$.

Eqn. 4.2 may be written in terms of C

$$L(r) \to \ln\left(\frac{r}{r_a}\right) - \frac{1}{2C}$$

Thus for positions near the wire

$$P(r) = V_a(1 - C\ln(r/r_a)^2)$$

This is, as expected, of coaxial form, Eqn. 2.4. The anode charge $q_a(t)$ is then given by Eqn. 2.6 with C as defined above.

4.3 Potential, field and capacitance in multiwire chambers

4.3.1 Potential distribution

Fig. 4.2. illustrates schematically the essential geometry of a standard MWPC, (in most practical situations $h_1 = h_2$).

The potential distribution $P_W(x, y)$ due to the anode wires being at unit potential may be written, formally, from Eqn. 4.1 of the previous section.

$$P_W(x, y) = -\sum_n C_n L_n(x, y, x_n, y_n) \tag{4.5a}$$

$$L_n(x, y, x_n, y_n) = \ln\left\{\frac{\cosh a(x - x_n) - \cos a(y - y_n)}{\cosh a(x - x_n) + \cos a(y + y_n - d)}\right\}^{1/2} \tag{4.5b}$$

where $a = \pi/2h, \quad h = (h_1 + h_2)/2 \quad$ and $\quad d = h_1 - h_2$.
The summation is taken over all anode wires, and the coordinates of the nth wire are (x_n, y_n). It is generally convenient, but not essential, to choose axes so that $y_n = 0$ and $x_0 = 0$, as shown in Fig. 4.2. It is also normal to employ constant wire pitch s, so that $x_n = ns$, and constant wire radius r_a. These conditions will be assumed below.

The unknown quantities $C_n (= q_n/2\pi\epsilon_0)$ may be found in the following manner. Let us express the potential, unity, at the mth wire surface. That is $x \to x_m$ and $y \to y_m$. Then

$$1 = -\sum_n C_n L_{nm} \tag{4.6}$$

where

$$L_{nm} = \ln\left\{\frac{\cosh as(m - n) - 1}{\cosh as(m - n) + \cos ad}\right\}^{1/2} \qquad n \neq m \tag{4.7a}$$

and

$$L_{mm} = \ln\frac{ar_a/2}{\cos(ad/2)} \qquad n = m \tag{4.7b}$$

Thus knowing the coefficients L_{nm}, the unknown vector C_n can be found by matrix inversion of Eqn. 4.6. (This process requires only the most modest computing power for any normal number of wires. Several inversion routines are available in the NAG library.)

For a symmetrical chamber $h_1 = h_2$ or $d = 0$. Then

$$L_{nm} = \ln|\tanh as(m - n)/2| \qquad n \neq m \tag{4.8a}$$

$$L_{mm} = \ln(ar_a/2) \qquad n = m \tag{4.8b}$$

4.3.2 Capacitance per unit length of anode wire

Suppose that the anode contains a large number of wires and that its total width is large compared with h_1 and h_2. Then in the central region, near the axes origin, the quantities C_n are constant, equal to C_0 say. From Section 4.2.1, $C_0 = q_0/2\pi\epsilon_0$ where q_0 is the charge per unit length of anode wire, the wire being at unit potential. The capacitance per unit length of wire is therefore $2\pi\epsilon_0 C_0$.

From Eqn. 4.6, since $C_n = C_0$ =constant,

$$1 = -C_0 \sum_n L_{n0} \tag{4.9}$$

where

$$L_{n0} = \ln \left\{ \frac{\cosh ans - 1}{\cosh ans + \cos ad} \right\}^{1/2} \qquad n \neq 0 \tag{4.10a}$$

$$L_{00} = \ln \left\{ \frac{ar_a/2}{\cos(ad/2)} \right\} \qquad n = 0 \tag{4.10b}$$

Following our now standard convention, Sections 3.1 and 4.3, we express the capacitance per unit length of wire as $C_1 = 4\pi\epsilon_0 C$ and define an effective cathode radius r_c through $C = 1/\ln(r_c/r_a)^2$. Then

$$C = -1/2 \sum_n L_{n0} \tag{4.11a}$$

and therefore

$$\ln r_c = \ln(4h/\pi) - 2\sum_1^\infty L_{no} \tag{4.11b}$$

For a symmetrical chamber $L_{n0} = \ln\tanh(n\pi s/4h)$, $n \neq 0$.

The general expression for r_c, Eqn. 4.11, may be compared with those for the two limiting cases.

Eqn. 4.3, for	$s \gg h$	$r_c = 4h/\pi$
Eqn. 3.2, for	$\cosh 2\pi h/s \gg 1$	$r_c = (s/2\pi)e^{\pi h/s}$

4.3.3 Field formulae

Field calculations are required to determine ion, and electron, trajectories. These may be found by partial differentiation of Eqn. 4.5. The rather clumsy results may be written

$$-\frac{\partial P_W}{\partial x} = \frac{a}{2}\sum_n C_n \frac{\sinh\theta_x(\cos\theta_d + \cos\theta_y)}{(\cosh\theta_x - \cos\theta_y)(\cosh\theta_x + \cos\theta_d)} \tag{4.12a}$$

$$-\frac{\partial P_W}{\partial y} = \frac{a}{2}\sum_n C_n \frac{\sin\theta_y(\cosh\theta_x + \cos\theta_d) + \sin\theta_d(\cosh\theta_x - \cos\theta_y)}{(\cosh\theta_x - \cos\theta_y)(\cosh\theta_x + \cos\theta_d)} \tag{4.12b}$$

where

$$\theta_x = a(x - x_n), \quad \theta_y = a(y - y_n), \quad \theta_d = a(y + y_n - d). \tag{4.12c}$$

4.3.4 Cathode at finite potential

Suppose the upper cathode in Fig. 4.2 is not grounded but instead at a potential V_c. (In the analyses below it is convenient to write $V_c = V_R V_a$, where V_a is the anode voltage.) This situation is easily treated as follows.

The potential $P_c(x, y)$ due to the upper cathode alone, the anode wires being absent, is given by

$$P_c(x, y) = V_R V_a (y + h_2)/(h_1 + h_2) \tag{4.13}$$

The potential due to the anode wires is, Eqn. 4.5,

$$P_W(x, y) = -V_a \sum_n C_n L_n(x, y, x_n, y_n)$$

The resultant potential is thus

$$P(x, y) = V_a \left[-\sum_n C_n L_n + V_R \left(y + h_2 \right) / \left(h_1 + h_2 \right) \right] \tag{4.14}$$

The quantities C_n are of course as yet unknown; they are determined not only by the applied anode voltage V_a but also by the charge induced on the anode wires by the cathode voltage V_c. The vector C_n may be found by the same method as employed in Section 4.3.1.

At the anode wire surfaces $P = V_a$. Thus, as in Section 4.3.1, let $x \to x_m$, $y \to y_m$. Then

$$1 - V_R(y + h_2)/(h_1 + h_2) = -\sum_n C_n L_{nm} \tag{4.15}$$

Where the matrix elements L_{nm} have been given in Eqn. 4.7. Thus the vector of quantities C_n may be found by (numerical) inversion of the matrix equation (4.15). The potential distribution may then be calculated from Eqn. 4.14.

The field components are clearly given by

$$E_x = -V_a \frac{\partial P_W}{\partial x} \tag{4.16a}$$

$$E_y = V_a \left[-\frac{\partial P_W}{\partial y} - \frac{V_R}{(h_1 + h_2)} \right] \tag{4.16b}$$

where the differential coefficients have been given in Section 4.3.3.

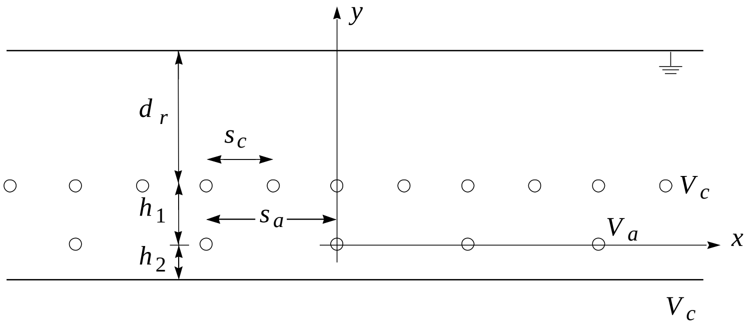

Figure 4.3

4.3.5 Chamber with drift region

A very important configuration is shown in Fig. 4.3, where a drift region of depth d_r precedes the chamber proper. It is generally convenient to operate the (conducting) window of the drift region at zero potential, with the cathodes at positive potential $V_c = V_R V_a$, and the anode at more positive potential V_a. The anode and cathode wire pitches are assumed constant at s_a and s_c respectively and the radii are also constants at r_a and r_c respectively. (Note the changed use of symbol r_c in this section.)

The potential and field distributions in this geometry may be found by exactly the same method as used in Sections 4.3.1 and 4.3.2. The resultant potential $P(x, y)$ is the sum of three components, due to the anode wires $V_a P_W$, the upper cathode wires $V_a P_{C_1}$, and the lower cathode $V_a P_{C_2}$.

$$P(x, y) = V_a(P_W + P_{C_1} + P_{C_2}) \tag{4.17}$$

Here, for the anode wires, from Eqn. 4.5,

$$P_W = -\sum_n C_n L_n(x, y, n) \tag{4.18a}$$

where

$$L_n = \ln \left\{ \frac{\cosh a(x - ns_a) - \cos ay}{\cosh a(x - ns_a) + \cos a(y - d)} \right\}^{1/2} \tag{4.18b}$$

$$a = \pi/(h_1 + h_2 + d_r), \quad d = h_1 - h_2 + d_r$$

For the cathode wires

$$P_{C_1} = -\sum_i C_i L_i(x, y, i) \tag{4.19a}$$

where

$$L_i = \ln\left\{\frac{\cosh a(x - is_c) - \cos a(y - h_1)}{\cosh a(x - is_c) + \cos a(y + h_1 - d)}\right\}^{1/2} \qquad (4.19b)$$

For the lower cathode

$$P_{C_2} = V_R(h_1 + d_r - y)/(h_1 + h_2 + d_r) \qquad (4.20)$$

The unknown quantities C_n, C_i may be determined by the standard method (Section 4.3.1). That is, numerical inversion is required of the matrix equation

$$P_j - P_C = -\sum_k C_k L_{kj} \qquad (4.21)$$

where, for summation over the anode wires,

$$P_j = 1 \qquad (4.22a)$$

$$P_C = V_R(h_1 + d_r)/(h_1 + h_2 + d_r) \qquad (4.22b)$$

$$L_{kj} = \ln\left\{\frac{\cosh a(k - j)s_a - 1}{\cosh a(k - j)s_a + \cos ad}\right\} \quad k \neq j \qquad (4.22c)$$

$$= \ln\left\{\frac{a_r/2}{\cos(ad/2)}\right\} \quad k = j \qquad (4.22d)$$

For summation over the cathode wires

$$P_j = V_R \qquad (4.23a)$$

$$P_C = V_R d_r/(h_1 + h_2 + d_r) \qquad (4.23b)$$

$$L_{kj} = \ln\left\{\frac{\cosh a(k - j)s_c - 1}{\cosh a(k - j)s_c + \cos a(2h_1 - d)}\right\}^{1/2} \quad k \neq j \qquad (4.23c)$$

$$= \ln\left\{\frac{ar_c/2}{\cos a(h_1 - d/2)}\right\} \quad k = j \qquad (4.23d)$$

Thus the LHS vector $(P_j - P_C)$ and the coefficients L_{kj} of the matrix equation 4.21 are all known. The vector C_k can therefore be found by (numerical) inversion. Hence the potential distribution can be determined from Eqn. 4.17. Partial differentiation of Eqn. 4.17. yields the two field components.

This section is particularly important since, not only can ion trajectories be determined [3], but also the primary electron trajectories (ignoring diffusion) from the drift region to the avalanche region. These latter calculations have proved useful in determining the significance of cathode wire pitch and registration [4].

It is clear that the present method may be easily adapted to find the induced charge on any single wire (see Section 4.4.3) or group of wires. In Chapter 5 it will be employed to determine the distribution of the induced charge on the wire cathode.

4.4 Anode charge waveforms

4.4.1 Coaxial region approximation

In typical MWPC geometry the number of anode wires is large (50–200) and the lateral width of the anode is large compared with the anode, cathode spacings. Under these (normal) conditions the argument of Section 4.3.2 may be employed to write the general expression for potential, Eqn. 4.5, in the somewhat simpler form

$$P_W(x,y) = -2C\sum_n L_n(x,y,n) \tag{4.24}$$

Here L_n is given by Eqn. 4.5b, with $x_n = ns$ and $y_n = 0$, and C by Eqn. 4.11a.

Now consider the region near the central, avalanche, anode wire and let $x \to 0$, $y \to 0$ with $(x^2+y^2)^{1/2} = r$. Eqn. 4.24 may now be written

$$P_W(r) = -2C\left\{\sum_{n\neq 0} L_{n0} + \ln\frac{ar/2}{\cos(ad/2)}\right\} \tag{4.25}$$

The quantities L_{n0} have been defined in Eqn. 4.10.
Eqn. 4.25 may therefore be written

$$P_W(r) = -2C\left\{\sum_n L_{n0} + \ln\frac{r}{r_a}\right\} \tag{4.26}$$

But, from Eqn. 4.11a, $\sum_n L_{n0} = -1/2C$.
Hence

$$P_W(r) = 1 - C\ln(r/r_a)^2$$

The potential distribution close to the anode wire is, as expected coaxial, with C given by the formulae in Section 4.2.2.

The anode charge waveform, under these conditions, therefore has the Wilkinson form, Eqn. 2.12.

$$q_a(t) = -q_0 C \ln(1 + t/t_0)$$

4.4.2 General case

Just as already described in Section 3.5.2, if signal processing time constants are relatively long enough that the ions have moved from the coaxial region then the anode and cathode waveforms must be constructed numerically. That is

$$q_a = -q_0[1 - P_W(x, y)]$$

where $P_W(x, y)$ is one of the various expressions developed in Section 4.3. The determination of q_c is described in Section 4.5.

The method of constructing the ion trajectory $x(t), y(t)$ has already been described in Section 3.3.2.

4.4.3 Induced charge on isolated anode wire

By measuring the charge induced on the anode wires adjacent to the avalanche wires it has been possible to study quantitatively the angular localisation of the avalanche [5]. The standard theoretical methods of this section may be applied to calculate the induced charge on a single anode wire, or indeed on any chamber wire.

Consider the chamber of Fig. 4.2 and suppose we wish to determine the charge induced on the kth wire. According to Eqn. 1.4 we need to evaluate $P_K(x, y)$, the potential due to the kth anode wire being at unit potential, all other wires and the chamber cathodes being grounded. Thus we must determine the vector C_n by inversion of the matrix equation

$$P_m = -\sum_n C_n L_{nm} \tag{4.27}$$

where $P_m = 0$, $m \neq k$ and $P_m = 1$, $m = k$. The coefficients L_{mn} have been defined in Eqn. 4.7. The signal charge induced on the kth anode wire by point charge q_0 at (x, y) is then

$$q_k(x, y) = q_0 P_K \tag{4.28a}$$

where

$$P_K(x, y) = -\sum_n C_n L_n(x, y, n) \tag{4.28b}$$

Of course if the kth wire is the avalanche wire then it will have collected a negative (electron) charge $-q_0$. The net charge is then $q_k = -q_0(1 - P_K)$.

4.5 Cathode charge waveforms

4.5.1 Continuous cathodes

The standard methods may be applied here. That is we wish to find the potential distribution $P_C(x, y)$ due to unit potential on the appropriate cathode, all other chamber electrodes being grounded. Consider the asymmetric chamber of Fig. 4.2 and suppose we wish to determine the signal charge q_c induced on the top electrode by a point charge q_0 at (x, y).

Unit potential on the top cathode induces charge (at present unknown) on the grounded anode wires. Thus, employing Eqn. 4.5, we may write

$$P_C(x, y) = -\sum_n C_n L_n(x, y, n) + (y + h_2)/(h_1 + h_2) \qquad (4.29)$$

The unknown quantities C_n may be determined from the condition that the anode wire surfaces are at zero potential.

$$-h_2/(h_1 + h_2) = -\sum_n C_n L_{nm} \qquad (4.30)$$

where the coefficients L_{nm} have been given in Eqn. 4.7. Inversion of the matrix equation 4.30 yields the vector C_n, so that P_C can be calculated from Eqn. 4.29. Then

$$q_c = q_0 P_C$$

The determination of the ion trajectory $x(t), y(t)$ is of course a separate calculation, as already described in previous sections.

Experimental measurement and theoretical calculations agree in showing the very strong dependence of q_c on initial ion angle α [6]. It is generally possible, by using the cathode signals, to discriminate very clearly between 'near-side' events and 'far-side' events [3].

4.5.2 Wire cathode

The procedure described in Section 4.4.3 for calculating the charge induced on an anode wire can obviously be applied also to any cathode wire, or group of cathode wires. Thus the distribution of charge on a wire cathode may be readily evaluated [2,3]. This topic is of considerable importance in considering the performance of position-sensitive detectors. The next chapter will deal in detail with the calculation of cathode charge distributions in MWPCs.

4.6 Approximation to the microstrip avalanche chamber (MAC)

The electrostatics of the MAC [7] should correctly be dealt with by one of the generalised computer packages now becoming more widely available. Nevertheless it is possible to apply the methods of this present section to make approximate but very simple, calculations of fields and ion trajectories. These calculations allow quantitative, physical insight into MAC operation and may indeed be quite adequate for certain purposes.

The overall geometric structure of the MAC consists of a conducting window plane, a gas-filled drift region, an active plane and a conducting back-electrode plane. The essential feature of the MAC is the active plane which consists of parallel microstrip alternating anodes and cathodes deposited on an insulating substrate. The anode pitch is very small, of the order 200μm, with microstrip anode width 5–10μm. Successful fabrication, and operation, of this structure has been made possible by the developments of electron beam lithography, allowing electrode dimensions to be determined to an accuracy of the order 0.1μm.

Primary electrons from the drift region avalanche in the high field close to a microstrip anode, the resulting positive ions travelling, mainly, to the two adjacent cathodes. The back electrode, at anode potential, is essential to prevent charging of the insulating substrate surface. The advantages of the MAC are seen as very high speed operation, due to the short ion collection times, and the possibility of high spatial resolution due to the very small anode pitch. The disadvantages are firstly the presently low gas gains attainable ($\sim 10^3$) and, secondly, the difficulty of obtaining good positional information parallel to the microstrip electrodes. This latter results from the necessarily very small signals induced on the back electrode and window, (see accompanying table).

Fig. 4.4 shows schematically, but not to scale, the multiwire structure that may be used to simulate, approximately, ion motion in a MAC. The anode strips have been replaced by anode wires, and the cathode strips by closely spaced cathode wires of very small radii. The relative dielectric constant of the substrate has been assumed to be unity. This last assumption represents the most serious approximation and will certainly affect absolute values of field. Nevertheless, provided this limitation is not forgotten, some instructive, guiding information can be obtained from this simple model.

The calculations of potential, field and ion trajectories follow the standard procedures already described in Sections 4.3.1, 4.3.2 and 4.4.3. The basic equation for potential, Eqn. 4.5 may be employed directly, remembering of course that in the present application neither the wire pitch

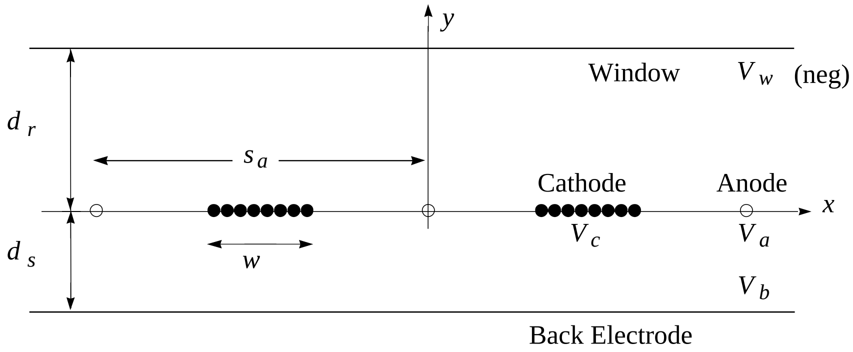

Figure 4.4

nor the wire radii are constants. Nor are all the wires in the active plane at the same potential. It is nevertheless a straightforward procedure to calculate the signal charges on each of the chamber electrodes, and indeed on each individual cathode wire. This latter calculation yields directly the distribution of induced charge across each cathode 'strip'. (This distribution of course varies with time but is found always to peak strongly on the wires closest to the anode wire.)

Two examples of the application of this model may illustrate its usefulness. The following parameters were employed for those particular calculations.

anode wire pitch,	s_a	200μm	anode voltage,	V_a	0.5kV
cathode width,	w	45μm	cathode voltage,	V_c	0.0kV
drift depth,	d_r	2.0mm	window voltage,	V_w	-1.0kV
substrate thickness,	d_s	0.5mm	back-electrode voltage,	V_b	0.5kV

Table 4.1 shows relative signal charges on the anode, the two adjacent cathodes and the back-electrode. These calculations were made assuming

Table 4.1

t [ns]	q_a	q_c	q_b
20	-0.472	0.366	0.0255
40	-0.563	0.440	0.0295
60	-0.626	0.498	0.0277
80	-0.702	0.586	0.0222
100	-0.744	0.636	0.0193

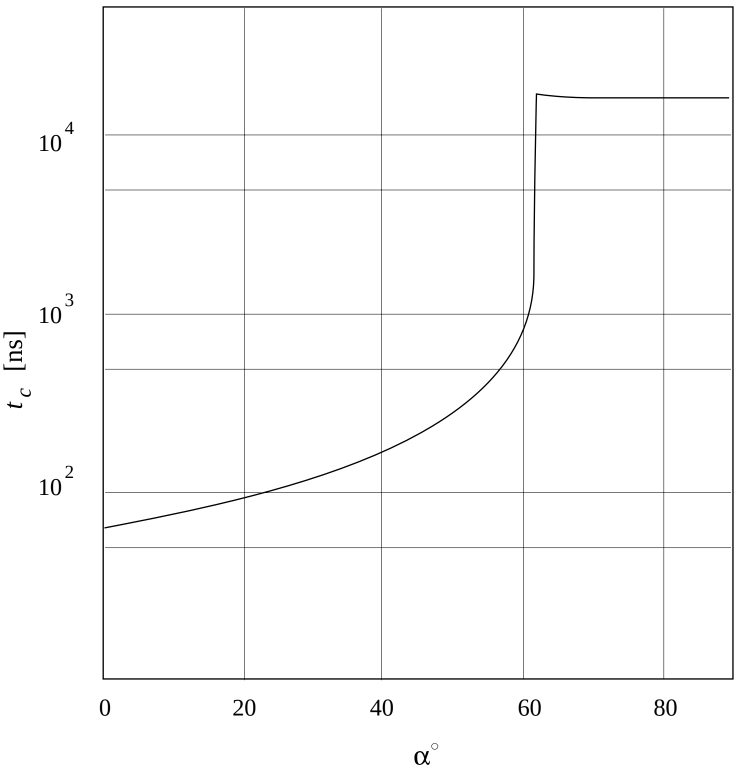

Figure 4.5

that the avalanche was distributed uniformly round the upper half of the anode wire. That is, each avalanche resulted in an equally weighted ‘fan’ of positive ions distributed, initially, uniformly round 180°. Of course the real avalanche distribution is not known.

The extremely rapid rise-times of the anode and cathode signal charges should be noted. Note also the very small charge induced on the back-electrode.

Fig. 4.5 shows ion collection time as a function of initial angle α at the anode wire surface. (Note the logarithmic scale of the time axis.) This curve shows that the majority of the ions generated in a uniformly distributed avalanche are collected very rapidly. The abrupt step near 62° represents the switch to collection by the window.

The field lines for this particular geometry and electrode voltages are shown in Fig. 4.6, and correspond to $\alpha = 0^\circ$ to 180° at 5° intervals.

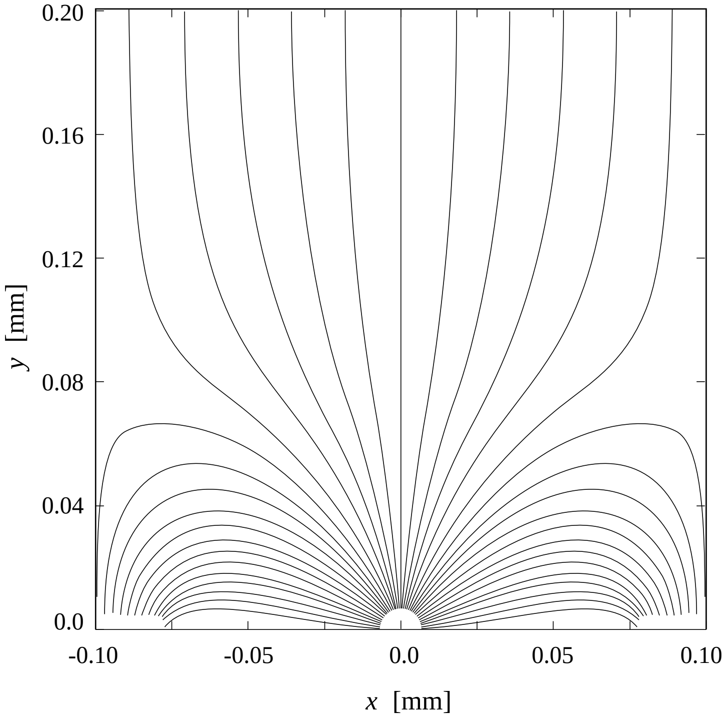

Figure 4.6

4.7 Alternative approach

In the rare circumstance that a matrix inversion library programme is not available, or if simplicity in coding and high speed operation are of particular importance, then, under certain restricted conditions, some of the problems treated in this chapter can be treated in a simpler manner.

Suppose that the number of anode wires is large $(50-100)$, that the lateral width of the anode is large compared with the anode, cathode spacing and that the anode, and cathode, wire pitches and radii are constants. This represents normal MWPC geometry. Then, provided the avalanche wire is not too near the edges of the anode plane, the quantities C_n in Eqn. 4.5 may be regarded as constant. Under these conditions, potential distributions can be obtained from simple summations only.

It must be stressed that this simplified approach cannot be employed to deal with the non-uniform situations treated in Sections 4.4.3 and 4.6, and all those treated in Chapter 5.

4.7.1 Anode charge in standard geometry, Fig. 4.2

It has already been shown in Sections 4.3.2 and 4.4.1 that if C_n can be regarded as constant then the potential function due to the anode at unit potential can be written, Eqn. 4.24,

$$P_W(x,y) = -2C\sum_n L_n(x,y,n) \tag{(4.24)}$$

where

$$C = -1/2\sum_n L_{n0} \tag{(4.11a)}$$

and L_{n0} has been defined in Eqn. 4.10. Then

$$q_a(x,y) = -q_0[(1 - P_W(x,y)]$$

In this case the ion trajectory $x(t)$, $y(t)$ can also be calculated from P_W (or rather from the differentials of V_aP_W).

4.7.2 Cathode charge in standard geometry, Fig. 4.2

In this case the potential $P_C(x,y)$ due to the upper cathode being at unit potential, the other electrodes being grounded, may be written, Eqn. 4.29, with $C_n = C_0 =$ constant,

$$P_C(x,y) = -C_0\sum_n L_n(x,y,n) + (y+h_2)/(h_1+h_2) \tag{4.31}$$

The constant C_0 is determined from the condition that the anode wire surfaces are at zero potential. Thus considering the wire at the coordinate origin

$$0 = -C_0\sum_n L_{n0} + h_2/(h_1+h_2)$$

Hence, using Eqn. 4.11a,

$$C_0 = -2Ch_2/(h_1+h_2)$$

Therefore

$$P_C(x,y) = 2C\frac{h_2}{h_1+h_2}\sum_n L_n(x,y,n) + \frac{y+h_2}{h_1+h_2} \tag{4.32}$$

and

$$q_C(x,y) = q_0P_C(x,y)$$

It is easily confirmed that Eqns. 4.24 and 4.32 reduce, when $x, y \ll s$, to the limiting forms Eqn. 3.3 and 3.6 respectively.

The ion trajectory $x(t), y(t)$ must of course be calculated from P_W, Eqn. 4.24.

4.7.3 Chamber with drift region, Fig. 4.3

This situation has been described in Section 4.2.5. The potential function due to the applied electrode potentials is, Eqn. 4.17.

$$P(x,y) = V_a(P_W + P_{C_1} + P_{C_2}) \tag{(4.17)}$$

Under the present conditions, for the anode wires,

$$P_W = -C_A \sum_n L_n(x,y,n)$$

and for the cathode wires,

$$P_{C_1} = -C_C \sum_i L_i(x,y,i)$$

P_{C_2} is given by Eqn. 4.20.

The two unknowns C_A and C_C may be obtained from the conditions that at the anode wire surfaces $P = V_a$ and at the cathode wire surfaces $P = V_R V_a$. These conditions may be written

$$1 - V_R(h_1 + d_r)/(h_1 + h_2 + d_r) = -C_A \sum_n L_{n0} - C_i \sum_i L_{iA} \tag{4.33}$$

$$V_R - V_R d_r/(h_1 + h_2 + d_r) = -C_A \sum_n L_{nC} - C_i \sum_i L_{i0} \tag{4.34}$$

The four summation elements in these two simultaneous equations may be written

$$L_{n0} = \ln\left\{\frac{\cosh ans_a - 1}{\cosh\ ans_a + \cosh ad}\right\}^{1/2} \qquad n \neq 0 \quad (4.35a)$$

$$= \ln\left\{\frac{ar_a/2}{\cos(ad/2)}\right\} \qquad n = 0 \quad (4.35b)$$

$$L_{i0} = \ln\left\{\frac{\cosh ais_c - 1}{\cosh ais_c + \cos a(2h_1 - d)}\right\}^{1/2} \quad i \neq 0 \qquad (4.36a)$$

$$= \ln\left\{\frac{ar_c/2}{\cos a(h_1 - d/2)}\right\} \qquad i = 0 \qquad (4.36b)$$

$$L_{nC} = \ln\left\{\frac{\cosh ans_a - \cos ah_1}{\cosh ans_a + \cos a(h_1 - d)}\right\}^{1/2} \qquad (4.37)$$

$$L_{iA} = \ln\left\{\frac{\cosh ais_c - \cos ah_1}{\cosh ais_c + \cos a(h_1 - d)}\right\}^{1/2} \qquad (4.38)$$

Thus having determined C_A and C_C from the two simultaneous equations 4.33 and 4.34 the potential $P(x, y)$ can be calculated from Eqn. 4.17.

References

1. E. Mathieson & T.J. Harris, Nucl. Instr. & Meth. 154 (1978) 189.
2. E. Mathieson, Nucl. Instr. & Meth. 159 (1979) 29.
3. J.S. Gordon & E. Mathieson, NuclInstr. & Meth. 227 (1984) 267.
4. E. Mathieson & G.C. Smith, IEEE Trans. Nucl. Sci. NS-37 (1990) 187.
5. T.J. Harris & E. Mathieson, Nucl. Instr. & Meth. 154 (1978) 183.
6. E. Mathieson & T.J. Harris, Nucl. Instr. & Meth. 159 (1979) 483.
7. A. Oed, Nucl. Instr. & Meth. A263 (1988) 351.

Chapter 5.

MULTIWIRE GEOMETRY III. Cathode charge distributions

A knowledge of the distribution of cathode induced charge is of importance in the prediction of performance of position-sensitive detection systems. There are a sufficient number of aspects of this interesting topic that they are most conveniently collected together in this separate chapter.

5.1 Exact distribution. Wire cathode

This geometry, see Fig. 4.3, has already been studied in Section 4.3.5, and indeed most of the formulae required for the present problem have been established there, and in Section 4.4.3. Following our standard procedure, in order to find the signal charge q_m induced, by unit point charge at (x, y), on the mth wire of the system we need to find the potential $P_M(x, y)$ due to that wire at unit potential all other wires and electrodes in the chamber being grounded. Thus, from Section 4.3.5,

$$P_M(x, y) = -\sum_m C_m L_m(x, y, m) \tag{5.1}$$

where $L_m(x, y, m)$ has been given in Eqns. 4.18 and 4.19, the sum being taken over both anode and cathode wires. The unknown vector of quantities C_m may be determined by inversion of the matrix equation

$$P_j = -\sum_k C_k L_{kj}$$

where $P_j = 1$ for $j = m$ and $P_j = 0$ for all other j. The coefficients L_{kj} have been given in Eqns. 4.22 and 4.23. Thus

$$q_m(x, y) = P_M(x, y)$$

The ion trajectory $x(t), y(t)$ may be determined by the method described in Section 3.3.2, but using of course the potential $P(x, y)$, Eqn. 4.17, derived in Section 4.3.5.

In practice it is convenient to calculate, and to measure experimentally, the ratio of signal charge induced on a cathode wire to the anode signal charge, $q_m(t)/q_a(t)$.

The distribution of induced charge on a wire cathode has been examined experimentally in considerable detail [1]; very close agreement was found with predictions of the above theory.

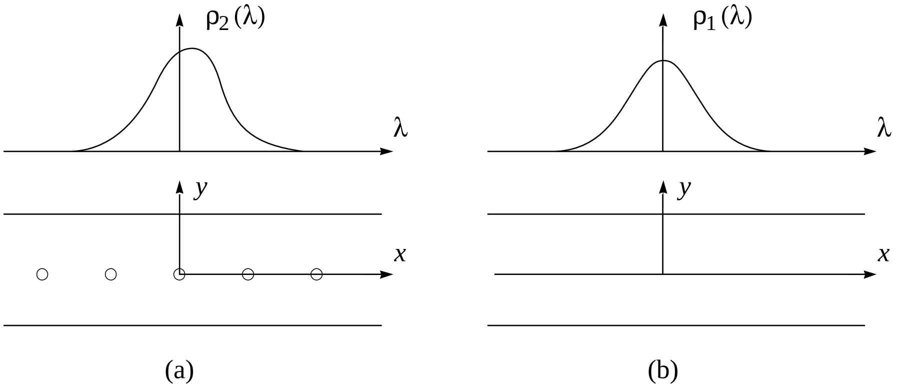

Figure 5.1

5.2 Exact distributions. Continuous cathode

In many position-sensitive detection systems the sensing cathode, although divided electrically into equal width strip, can be regarded as a continuous conducting plane. It becomes important for predicting performance, therefore, to determine the induced charge distribution on this plane.

It is found very convenient to employ normalised distance on the cathode, $\lambda = x/h$, where h is the anode, cathode spacing of the (symmetrical) chamber. Then $-\rho(\lambda)d\lambda$ is the charge induced on the upper cathode of the chamber, between λ and $\lambda + d\lambda$, by a unit point charge at (x, y).

Two geometries must be distinguished. In the first case the anode wires are normal to the x-axis, Fig. 5.1(a). For historic reasons the distribution normal to the x-axis will be denoted by $\rho_2(\lambda)$. In the second case the anode wires are parallel to the x-axis, Fig. 5.1(b). The distribution parallel to the anode wires will be denoted by $\rho_1(\lambda)$.

In practical situations it is very convenient to normalise the distribution $\rho(\lambda,\, t)$ to the magnitude of the net anode charge $|q_a(t)|$. Thus

$$\Gamma(\lambda,t) = \rho(\lambda,t)/|q_a(t)|$$

This distribution remains of course a function of time t but the gross variation with t has been removed.

5.2.1 Exact distribution ρ_2

Consider an infinitesimal strip of width $d\lambda$ on the upper cathode of Fig. 5.1(a), and suppose that this strip is at unit potential, the remainder of that cathode and all other electrodes in the chamber being grounded. Then if the potential distribution in the chamber under these conditions is

$dP_S(x, y, \lambda)$ then, by Eqn. 1.1, the charge induced on the strip by a unit point charge at (x, y) is $-dP_S(x, y, \lambda)$. Thus

$$-\rho_2(x, y, \lambda)d\lambda = -dP_S(x, y, \lambda)$$

or briefly,

$$\rho_2 = dP_S/d\lambda \tag{5.2}$$

The potential function dP_S may be found in the following way.

$$dP_S = dP_s + dP_w \tag{5.3}$$

where dP_s is the potential function due to the strip at unit potential, the anode wires being absent, and dP_w is the potential function due to the charge distribution induced on the anode wires by the strip.

It is shown in Appendix 3 that dP_s may be written

$$dP_s = \frac{1}{4}\frac{\cos ay}{\cosh a(x - h\lambda) - \sin ay}d\lambda \tag{5.4}$$

where $a = \pi/2h$.
The potential due to the induced anode charges may be written, Eqn. 4.5 with $d = 0$ and $y_n = 0$,

$$dP_w = -\sum_n dC_n L_n(x, y, n) \tag{5.5}$$

However each anode wire surface must be at zero potential. That is $dP_S \rightarrow 0$ as $x \rightarrow ms + r_a$, $y \rightarrow r_a$. Thus Eqn. 5.3 becomes

$$-\frac{1}{4}\operatorname{sech} a(ms - h\lambda) = -\sum_n \frac{dC_n}{d\lambda}L_{nm} \tag{5.6}$$

where the coefficient L_{nm} have been given in Eqn. 4.7 (with $d = 0$). The unknown vector $dC_n/d\lambda$ may thus be found by numerical inversion of the matrix Eqn. 5.6. Then, finally, from Eqn. 5.3,

$$\rho_2(\lambda) = \frac{1}{4}\frac{\cos ay}{\cosh a(x - h\lambda) - \sin ay} - \sum_n \frac{dC_n}{d\lambda}L_n(x, y, n) \tag{5.7}$$

5.2.2 Exact distribution ρ_1

In this section we will employ, for the only time in these multiwire studies, three-dimensional geometry. This analysis is an extension of that first presented by Gatti et al. [2].

The basic approach is of course the same as that employed in the previous section. However in this case the positive ion trajectory remains always in the plane $x = 0$. The charge induced on an infinitesimal cathode strip of width $d\lambda$ at λ by a unit charge at $(0, y, z)$, $-\rho_1(\lambda)d\lambda$, is from Eqn. 1.1, equal to the negative of the potential at $(0, y, z)$ due to that strip being at unit potential, the remainder of that cathode and all other electrodes being at zero potential. This potential function is necessarily an even function of λ and is therefore equal to the potential $dP_S(x, y, z)$ due to the unit potential strip $d\lambda$ being situated at $\lambda = 0$.
Thus

$$\rho_1(\lambda) = dP_S/d\lambda \tag{5.8}$$

where, as before

$$dP_S = dP_s + dP_w \tag{5.9}$$

dP_s is again given by Eqn. 5.4, but with $x = 0$.

The calculation of dP_w, however, is entirely different from that in the previous section. There the anode wire induced charge density was uniform along the length of the wire, although of course varying from wire to wire. In the present case the induced charge density now varies along the wires, but is the same function for all wires. Let us denote this charge density by dq. (The differential has been used, as in the previous section, since this charge distribution is induced by the infinitesimal strip of width $d\lambda$.) The charge induced on an infinitesimal length dx' at x' of each wire is $dq(x')dx'$.

We may now employ standard electrical image theory to write down a formal expression for the potential $dP_w(x, y, z)$ due to the induced anode charge.

$$dP_w = \sum_{k=-\infty}^{\infty} \sum_{n=-\infty}^{\infty} \int_{-\infty}^{\infty} \frac{dq(x')}{4\pi\epsilon_0} \frac{\cos \pi n}{\{(x - x')^2 + (y - 2nh)^2 + (z - ks)^2\}^{\frac{1}{2}}} dx' \tag{5.10}$$

The integer k represents the kth anode wire; the integer n represents the nth image of that wire.

Equation 5.10 may be re-written in terms of $\lambda = x/h$ and $\lambda' = x'/h$

$$dP_w/d\lambda = \int_{-\infty}^{\infty} f(\lambda')h(\lambda - \lambda')\, d\lambda' \tag{5.11}$$

where

$$f(\lambda) = \frac{1}{4\pi\epsilon_0} \frac{dq}{d\lambda} \tag{5.12}$$

$$h(\lambda) = \sum_k \sum_n \frac{\cos \pi n}{(\lambda^2 + b^2)^{\frac{1}{2}}} \tag{5.13}$$

and

$$b^2 = (y/h - 2n)^2 + (z/h - ks/h)^2 \tag{5.14}$$

The function $f(\lambda)$ is determined by the condition that the surfaces of the anode wires must be at zero potential. This condition may be written, to an excellent approximation ($r_a \ll s, h$), from Eqn. 5.9,

$$0 = \frac{1}{4}\operatorname{sech}\left(\frac{\pi\lambda}{2}\right) + \int_{-\infty}^{\infty} f(\lambda')h_0(\lambda - \lambda')\, d\lambda' \tag{5.15}$$

where

$$h_0(\lambda) = \sum_k \sum_n \frac{\cos \pi n}{(\lambda^2 + b_0^2)^{\frac{1}{2}}} \tag{5.16}$$

and

$$b_0^2 = (r_a/h)^2 + (2n)^2 + (ks/h)^2 \tag{5.17}$$

The convolution integral (5.15) shows that the Fourier transform $F(\omega)$ of $f(\lambda)$ is given by

$$F(\omega) = G_0(\omega)/H_0(\omega) \tag{5.18}$$

where

$$G_0(\omega) = -\frac{1}{2}\operatorname{sech}(\omega) \tag{5.19}$$

and

$$H_0(\omega) = \sum_k \sum_n 2\cos(\pi n)K_0(b_0\omega) \tag{5.20}$$

Here K_0 is the zero order of Bessel function of the second kind.

It now follows from the convolution integral Eqn. 5.11 that the Fourier transform of $dP_w/d\lambda$ is given by

$$G(\omega) = F(\omega)H(\omega) = G_0(\omega)H(\omega)/H_0(\omega) \tag{5.21}$$

where

$$H(\omega) = \sum_k \sum_n 2\cos(\pi n)K_0(b\omega) \tag{5.22}$$

Thus $dP_w/d\lambda$ can be found as the (numerical) transform of $G(\omega)$ given by Eqn. 5.21. Then

$$\rho_1(\lambda) = \frac{1}{4}\frac{\cos \pi y/2h}{\cosh \pi\lambda/2 - \sin \pi y/2h} + \frac{dP_w}{d\lambda} \tag{5.23}$$

It should be especially noted that the numerical evaluation of $H_0(\omega)$ and $H(\omega)$, Eqns. 5.20 and 5.22, require special attention if high accuracy is to be achieved. Full details of suitable procedures are given in Appendix 5 (and in ref. [3]).

5.3 Approximate distributions

Although the functions ρ_1 and ρ_2 determined in the two previous sections represent accurate descriptions of the cathode charge distributions, in many practical applications such detail is not required. Approximate distributions representing average behaviour may be more useful. This is particularly so if distributions independent of time can be formulated. The two sections below show how such average, time independent, distributions can be determined.

The approximations employed are basically the same for the two geometries. Having, as before, determined dP_w from the condition that $dP_s + dP_w = 0$ at the anode wire surfaces, the potential function near the anode wire is then approximated by dP_w alone. A further approximation for dP_w, valid for $r \ll s$, is then employed.

5.3.1 Approximate distribution ρ_2

The first term of Eqn. 5.9 is assumed negligible compared with the second. That is

$$\rho(\lambda)d\lambda = dP_w \tag{5.24}$$

In order to estimate dP_w recall, from Section 4.2.1, that the induced charge per unit length of an anode wire is $2\pi\epsilon_0 dC_n$. Thus, applying Gauss's theorem, the radial induced field close to the central anode wire is dC_0/r. Thus, since the wire surface is at zero potential, the potential function must be given by

$$dP_w = -dC_0 \ln(r/r_a) \tag{5.25}$$

Thus

$$\rho_2(\lambda) = -\frac{1}{2}\frac{dC_0}{d\lambda} \ln\left(\frac{r}{r_a}\right)^2 \tag{5.26}$$

For ions moving in the coaxial field region close to the avalanche wire the net anode signal has the simple form, Eqn. 2.6 with $q_0 = 1$,

$$q_a = -C \ln(r/r_a)^2 \tag{5.27}$$

where C has been defined in Section 4.3.2. Thus

$$\Gamma_2(\lambda) \equiv \frac{\rho_2(\lambda)}{|q_a|} = -\frac{1}{2C}\frac{dC_0}{d\lambda} \tag{5.28}$$

The quantity $dC_0/d\lambda$ must of course be determined by matrix inversion of Eqn. 5.6, despite the approximation implied by Eqn. 5.24.

It should be especially noted that $\Gamma_2(\lambda)$ is independent of r and hence of time t. The distribution is , naturally, an approximation; it cannot represent the effects of avalanche angular localisation.

A necessary condition to be met in any numerical evaluation of Γ_2 is that

$$\int_{-\infty}^{\infty} \Gamma_2(\lambda) d\lambda = \frac{1}{2} \tag{5.29}$$

This forms a valuable check on accuracy.

5.3.2 Approximate distribution ρ_1

The first term of Eqn. 5.2.3 is assumed negligible compared with the second. That is

$$\rho_1(\lambda) d\lambda = dP_w \tag{5.30}$$

where dP_w is the potential function due to the induced charge density dq. Applying Gauss's theorem, the induced field very close to an anode wire is $dq/2\pi\epsilon_0 r$, and, since the wire is at zero potential, the potential function must be given by

$$dP_w = -\frac{dq}{2\pi\epsilon_0} \ln\left(\frac{r}{r_a}\right) \tag{5.31}$$

or, from Eqn. 5.12,

$$dP_w = -2f(\lambda) d\lambda \ln\left(\frac{r}{r_a}\right)$$

Thus

$$\rho_1(\lambda) = -f(\lambda) \ln(r/r_a)^2 \tag{5.32}$$

Again, for ions moving in the coaxial field region close to the avalanche wire, the net anode signal has the simple form, Eqn. 2.6 with $q_0 = 1$,

$$q_a = -C \ln(r/r_a)^2$$

where C has been defined in Section 4.3.2. Thus

$$\Gamma_1(\lambda) \equiv \frac{\rho_1(\lambda)}{|q_a|} = -\frac{f(\lambda)}{C} \tag{5.33}$$

$f(\lambda)$ is obtained as the inverse Fourier transform of $F(w)$ given by Eqn. 5.18. As noted in Section 5.2.2, the evaluation of $H_0(w)$ requires special attention (see Appendix 5).

The function $\Gamma_1(\lambda)$ is independent of r and hence of time t. It is an approximation and cannot describe the effects of avalanche angular localisation.

An important check on accuracy in numerical evaluation of Γ_1 is the necessary condition

$$\int_{-\infty}^{\infty} \Gamma_1(\lambda) d\lambda = \frac{1}{2} \tag{5.34}$$

5.4 Limiting approximate distributions

It is of both theoretical and practical interest to examine the form of the approximate distributions Γ_1 and Γ_2 for the limiting situations, $s \gg h$ and $s \ll h$.

5.4.1 Approximate distribution, pill-box geometry

The pill-box counter has only a single wire and can be approximated by $s \gg h$. In this case there is only the central dominant term, $m = 0$, in the summation of Eqn. 5.6

$$\frac{1}{4}\operatorname{sech}\frac{\pi\lambda}{2} = \frac{dC_0}{d\lambda}\ln\left(\frac{\pi r_a}{4h}\right) \tag{5.35}$$

Further, as shown in Section 4.1, for this situation $s \gg h$,

$$C = 1/\ln(4h/\pi r_a)^2$$

Thus, from Eqn. 5.28,

$$\Gamma_2(\lambda) = \frac{1}{4}\operatorname{sech}\frac{\pi\lambda}{2} \tag{5.36}$$

A distribution proportional to $\operatorname{sech}(\pi\lambda/2)$ was first employed by Endo et al. [4]. Gatti et al. [2] have shown that in the limit $s \to \infty$ then $\rho_1(\lambda)$ also becomes proportional to $\operatorname{sech}(\pi\lambda/2)$. That is $\Gamma_1 = \Gamma_2$.

5.4.2 Approximate distribution, parallel plate geometry

If $s \ll h$ then geometry approaches parallel plate conditions; the anode plane tends to a continuous conducting surface. To preserve the symmetry of the system it must be assumed that the charge induced on the upper cathode is due to an avalanche producing 0.5 units of positive ion charge above the anode plane and 0.5 units below the plane. If the anode is a conducting plane at zero potential, the potential function due to an infinitesimal cathode strip of width $d\lambda$ at $\lambda = 0$ may now be written (see Appendix 3)

$$dP_s = \frac{1}{2}\frac{\sin\pi y/h}{\cosh\pi\lambda + \cos\pi y/h}d\lambda \tag{5.37}$$

For $y \ll h$

$$dP_s = \frac{\pi y}{4h}\operatorname{sech}^2\frac{\pi\lambda}{2}d\lambda$$

Thus the signal charge induced on an infinitesimal cathode strip of width $d\lambda$ at λ, by 0.5 units of charge at $(0, y)$, is given by

$$\rho(\lambda)d\lambda = \frac{\pi y}{8h}\operatorname{sech}^2\frac{\pi\lambda}{2}d\lambda \tag{5.38}$$

The net anode charge due to unit avalanche charge is, from Eqn. 1.2,

$$q_a = -y/h \tag{5.39}$$

Thus

$$\Gamma(\lambda) \equiv \frac{\rho(\lambda)}{|q_a|} = \frac{\pi}{8}\mathrm{sech}^2\frac{\pi\lambda}{2} \tag{5.40}$$

A distribution proportional to $\mathrm{sech}^2\pi\lambda/2$ was first proposed by Lee et al. [5].

5.5 Single parameter empirical formula

Although the approximate distributions of Section 5.3 may be determined very rapidly it is nevertheless more convenient for some practical applications to employ a simple empirical formula. For such purposes a three-parameter empirical formula was proposed by Gatti et al. [2]. In the present terminology this formula may be written

$$\Gamma(\lambda) = K_1\frac{1-\tanh^2 K_2\lambda}{1+K_3\tanh^2 K_2\lambda} \tag{5.41}$$

However in the present formulation the total signal charge induced on a cathode is 1/2. That is, Eqns. 5.29 and 5.34,

$$\int_{-\infty}^{\infty}\Gamma(\lambda)d\lambda = \frac{1}{2}$$

This condition shows that there are now only two independent parameters, K_2 and K_3.

$$K_1 = \frac{K_2K_3^{1/2}}{4\tan^{-1}K_3^{1/2}} \tag{5.42}$$

It is instructive, following the example of Gatti et al. [2], to form a table showing the three parameter values at the extreme limits of h/s. These values may be obtained from the limiting distributions Eqns. 5.36 and 5.40.

h/s	K_1	K_2	K_3
0	1/4	$\pi/4$	1
∞	$\pi/8$	$\pi/2$	0

Calculations have been made of Γ_1 and Γ_2, from Section 5.3, for a wide range of chamber geometries in order to find a simple empirical expression for K_2 in terms of K_3. Close fitting to the distribution (rms deviation of the order 0.1% or less of peak volume) has been obtained by the following relationship [6, 7]

$$K_2 = \frac{\pi}{2}\left(1 - \frac{1}{2}K_3^{1/2}\right) \tag{5.43}$$

This empirical expression for K_2 now allows the normalised distribution $\Gamma(\lambda)$, Eqn. 5.41, to be determined by the single parameter K_3.

The FWHM of the distribution may be written

$$\frac{FWHM}{h} = \frac{4\tanh^{-1}(2+K_3)^{-1/2}}{\pi(1-0.5K_3^{1/2})} \tag{5.44}$$

Values of K_3 as a function of chamber parameters h/s and r_a/s are shown in Figs. 5.2 and 5.3 (a) and (b). For small $h/s(\lesssim 1.0)$ the two empirical distributions Γ_1 and Γ_2 differ somewhat but great significance should not be attached to this; neither is correct!

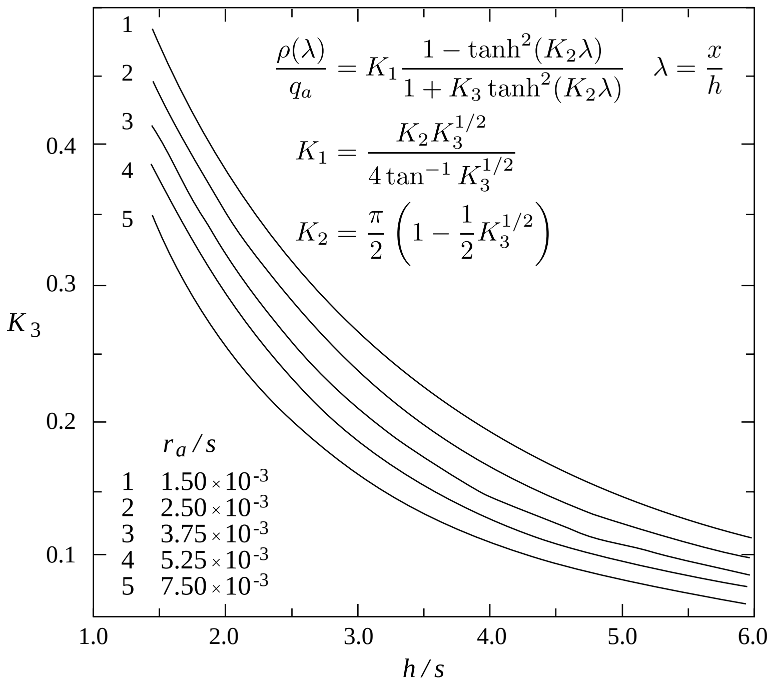

Figure 5.2

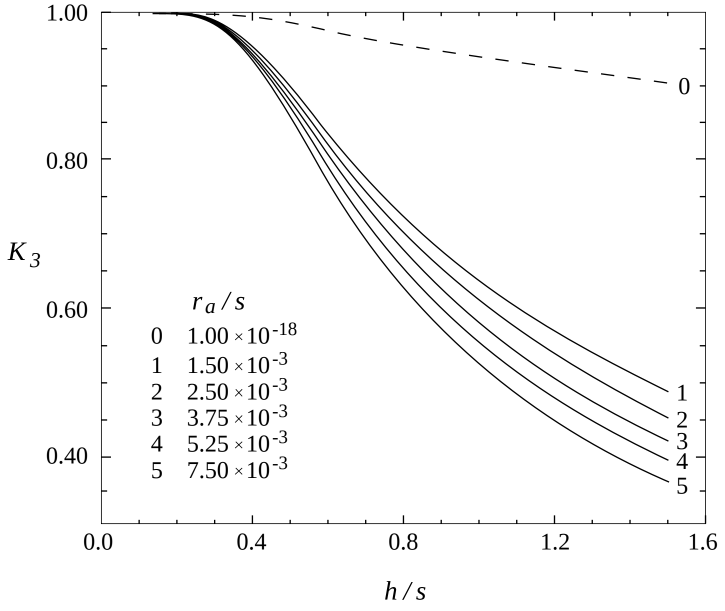

Figure 5.3(a)

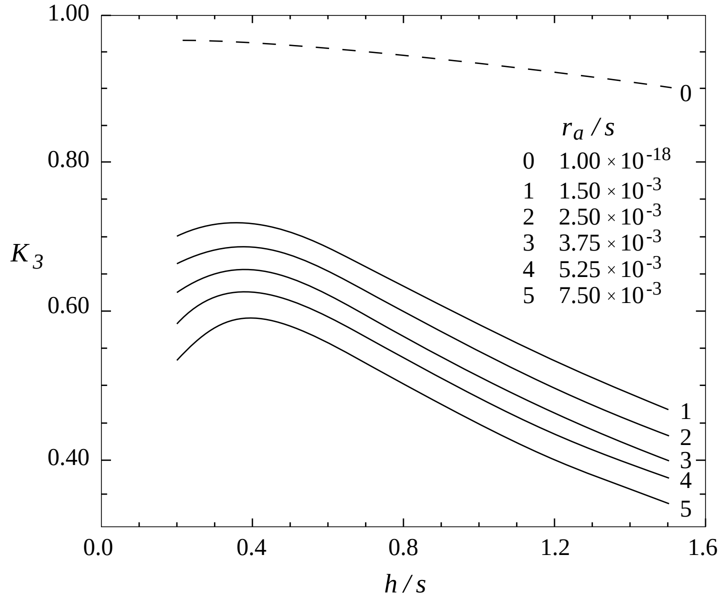

Figure 5.3(b)

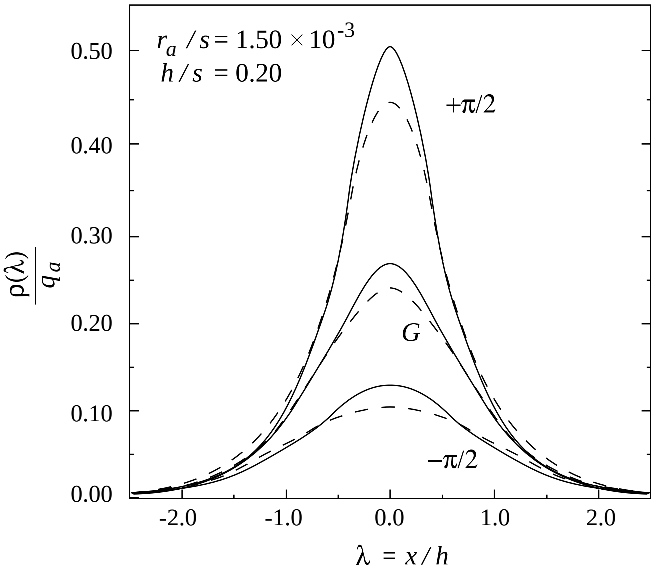

Figure 5.4 Comparison of empirical distributions, G, with exact distributions; ρ_1 (full curves) and ρ_2 (broken curves). The exact distributions were calculated at a time 1.0μs, for avalanche angular positions $\alpha = +\pi/2$ and $-\pi/2$, with rms angular spread $\sigma = 40°$, and for $s = 3.0$mm, $V_a = 0.8$kV and $\mu = 1.9\text{cm}^2/\text{V s}$. The total cathode charges, relative to the net anode charge, are -0.71 (ρ_1 and ρ_2) for $+\pi/2$, 0.29 for $-\pi/2$ and necessarily 0.5 for G. The empirical distributions represent $K_3 = 0.70$ for ρ_1 and 1.0 for ρ_2.

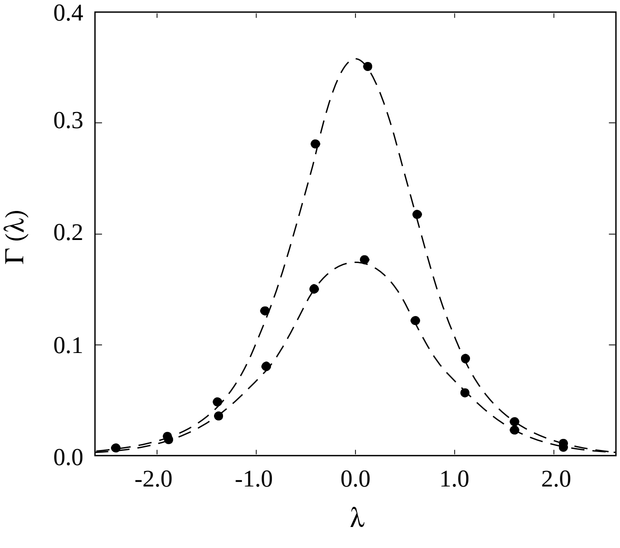

Figure 5.5

The use of Figs.5.2 and 5.3 and the empirical distribution Eqn. 5.41 should be of assistance in making estimates of differential non-linearity in position-sensitive MWPCs. In situations with small DFNL, say of the order 2% or less, this procedure should be of quite adequate accuracy. However its limitations should be borne in mind if a detailed description is essential. The cathode distributions for 'near-side' and 'far-side' avalanches differ in shape as well as in magnitude so that with some read-out systems, or near the edges of the field, double images can be generated. This behaviour can not be predicted by the 'average' distribution Eqn. 5.41. Some comparisons between exact and approximate distribution functions are shown in Fig. 5.4.

A typical comparison between experimental measurement of cathode charge distribution and theoretical prediction (as described in Section 5.1) is shown in Fig. 5.5. The two curves correspond to $\alpha = +\pi/2$, near-side events, and $\alpha = -\pi/2$, far-side events. The detailed conditions for these particular investigations are described in ref. [1].

References

1. J.S. Gordon & E. Mathieson, Nucl. Instr. & Meth. 221 (1984) 267.
2. E. Gatti, A. Longoni, H. Okuno & P. Semenza, Nucl. Instr. & Meth. 163 (1979) 83.
3. J.R. Thompson, J.S. Gordon & E. Mathieson, Nucl. Instr. & Meth. A234 (1985) 505.
4. I. Endo, T. Kawamoto, Y. Mizuno, T. Ohsugi, T. Taniguchi & T. Takeshita, Nucl. Instr. & Meth. 188 (1981) 51.
5. D. Lee, S. Sobottka & H. Thiessen, Nucl. Instr. & Meth. 104 (1972) 179.
6. E. Mathieson & J.S. Gordon, Nucl. Instr. & Meth. 227 (1984) 277.
7. E. Mathieson, Nucl. Instr. & Meth. A270 (1988) 602.

Chapter 6.

PARALLEL PLATE GEOMETRY
Anode and cathode charge distributions

6.1 Introduction

This chapter's contents are mainly a reproduction of ref. [14].

The development with time of the current in the external circuit of a parallel plate avalanche chamber (PPAC) is very well understood. Theoretical analyses have been presented by Schmidt [1] and Draper [2] and, in great detail, in the comprehensive study of Raether [3]. Understandably these early analyses were not concerned with the spatial distribution of the currents at the chamber electrodes. Experimentalists, however, soon realised the potential of the PPAC as a position-sensitive device so that, despite considerable technical difficulties, successful detectors have now been developed for localising X-rays, see for example refs. [4–8], and particles, see for example refs. [9,10].

Surprisingly, a simple theory of the spatial distribution of the charges appearing on the anode and cathode of a PPAC does not yet appear to have been presented. Such knowledge is necessary in estimating differential non-linearities and resolution in position-sensitive chambers. The essential feature of the present approach is that one obtains, analytically, the Fourier transform of the electrode charge distributions. Simple numerical inverse transformation then yields the actual distributions. This analysis is concerned mainly with X-ray detection but the method should be adaptable also to the case of particle radiation.

6.2 Theory

6.2.1 Basic formulae

The geometry for the present analysis is shown in Fig. 6.1. The cathode of the PPAC is a fine mesh or closely spaced wire grid which allows an electron swarm, from an ionising event in the drift region, to enter the high-field avalanche region. The locus of the centre-of-charge of the electron swarm defined the y-axis. The cathode is situated in the plane $y = h$ and the anode in the plane $y = 0$.

Under normal operating conditions the avalanche process is known to be completed very rapidly, within a few nanoseconds; in the present analysis it will be assumed that this time is always very small compared with any signal processing times and therefore can be regarded as effectively

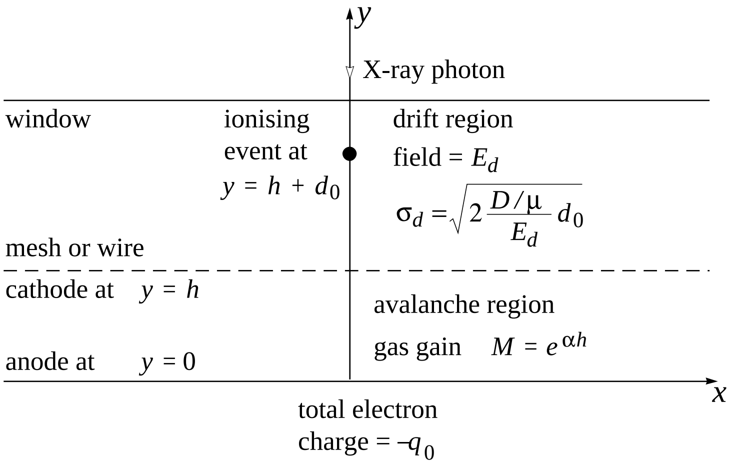
y
X-ray photon
window
ionising event at $y = h + d_0$
drift region
field = E_d
$\sigma_d = \sqrt{2\frac{D/\mu}{E_d}d_0}$
mesh or wire
cathode at $y = h$
avalanche region
gas gain $M = e^{\alpha h}$
anode at $y = 0$
x
total electron charge = $-q_0$

Figure 6.1 Geometry of parallel plate avalanche chamber, with drift region

zero. Change in the electrode charges after time $t = 0$ is then due to the relatively slow drift of the positive ions created in the avalanche. It will be assumed initially that the time taken for the electron swarm to cross the cathode plane is also zero; the modifications required to treat the case of finite crossing duration, tens of nanoseconds, will be discussed later.

Suppose a number N electrons enter the avalanche region in a very short time interval. Then, if α is the first Townsend coefficient, the number of electrons at distance y from the anode is $NM\exp(-\alpha y)$ where $M = \exp(\alpha h)$ is the mean gas gain. The linear charge density of positive ions created at $t = 0$ by the avalanche is therefore $\alpha q_0 \exp(-\alpha y)$, where $-q_0$ is the total electron charge arriving at the anode ($-q_0/M$ is the initial electron charge entering the avalanche region). Let the drift velocity of the positive ions be v, and, for convenience, define a total collection time $T = h/v$ (T is of the order tens of microseconds). Then after a time t the linear charge density of the ions becomes

$$p(y,t) = \alpha q_0 M^{-(y/h - t/T)}, \quad t/T \leq y/h \leq 1. \tag{6.1}$$

If $y/h < t/T$ then $p = 0$.

Let the charges induced on the anode and cathode surfaces by the positive ions be $-q_A$ and $-q_C$ respectively, and let the electron charge arriving at the anode and the positive ion charge arriving at the cathode be q_e and q_p respectively. Then the net, observable charge signals at the anode and cathode are q_a and q_c given by

$$q_a = q_A + q_e, \qquad q_c = q_C + q_p \tag{6.2.a, b}$$

It is readily shown that these charges are given by the following expressions

$$\frac{q_A}{q_0} = 1 - \frac{t}{T} - \frac{1 - M^{-(1-t/T)}}{\ln M}, \qquad \frac{q_e}{q_0} = -1, \tag{6.3a, b}$$

$$\frac{q_C}{q_0} = 1 - \frac{q_A}{q_0} - M^{-(1-t/T)}, \qquad \frac{q_p}{q_0} = \frac{M^{t/T} - 1}{M}. \tag{6.4a, b}$$

If, as is usual, $M \gg 1$ then these expressions reduce for the case $t \ll T$ to the well-known result $q_a/q_0 = -q_c/q_0 = -1/\ln M$.

6.2.2 Induced charge distributions

The analysis given in Appendix 3 shows that a unit point charge at x', y' induces electrode charge density ρ^0 (charge per unit width measured in the x-direction) given by

$$\rho^0_{A,C} = \frac{1}{2h} \frac{\sin \pi y'/h}{\cosh \pi (x - x')/h \mp \cos \pi y'/h}. \tag{6.5}$$

The negative sign in the denominator refers to the anode and the positive sign to the cathode.

Now we assume, with Raether [3], that the avalanche results in a positive ion distribution which has a Gaussian spread normal to the y-axis, the rms width increasing as the square root of the avalanche depth. Furthermore, after $t = 0$, this ion distribution drifts with uniform velocity h/T in the y-direction. That is, using Eqn. 6.1, the ion charge between the planes y' and $y' + dy'$ and between the planes x' and $x' + dx'$ at time t, is given by

$$p(x', y', t)dx'\, dy' = \alpha q_0 M^{-(y'/h - t/T)} \frac{1}{\sqrt{2\pi\sigma_y^2}} e^{-x'^2/2\sigma_y^2} dx'\, dy', \tag{6.6}$$

where

$$\sigma_y^2 = \sigma_A^2 (1 - y'/h + t/T). \tag{6.7}$$

Here σ_A is the rms spread of the electron avalanche at the anode. If $y'/h < t/T$ then $p(x', y', t) = 0$.

By multiplying Eqn. 6.6 by Eqn. 6.5 and integrating appropriately, formal expressions are obtained for the electrode induced charge distributions. Less clumsy nomenclature results if we now employ normalised quantities. That is, define $\lambda = x/h$, $\lambda' = x'/h$, $\theta = \pi y'/h$, $s_y = \sigma_y/h$ and

$\Gamma(\lambda) = \rho(\lambda)/q_0$, where $-\rho(\lambda)d\lambda$ is the charge induced on the electrode surface between λ and $\lambda + d\lambda$. Then, after some manipulation

$$\Gamma_{A,C}(\lambda, M, \frac{t}{T}) = \frac{\ln M M^{\frac{t}{T}}}{2\pi} \int_{\frac{\pi t}{T}}^{\pi} M^{-\frac{\theta}{\pi}} \int_{-\infty}^{\infty} \frac{e^{-\lambda'^2/2s_y^2}}{\sqrt{2\pi s_y^2}} \frac{\sin\theta}{\cosh\pi(\lambda-\lambda') \mp \cos\theta}\, d\lambda' d\theta \tag{6.8}$$

The inner integral, $S(\lambda)$ say, may be written

$$S(\lambda) = \frac{1}{2\pi} \int_{-\infty}^{\infty} F(k) H(k) \cos k\lambda \, dk, \tag{6.9}$$

where

$$F(k) = \exp(-k^2 s_y^2/2) \tag{6.10}$$

and

$$\begin{aligned} H(k) &= \int_{-\infty}^{\infty} \frac{\sin\,\theta \cos\,k\lambda}{\cosh\,\pi\lambda \mp \cos\,\theta}\, d\lambda \\ &= 2\frac{\sinh\,k(1-\theta/\pi)}{\sinh k} \qquad \text{for anode} \\ &= 2\frac{\sinh\,k\theta/\pi}{\sinh\,k} \qquad \text{for cathode.} \end{aligned} \tag{6.11}$$

The definite integral, Eqn. 6.11, may be found in (ref. [11] p.505). It is now possible to carry out the outer integration over θ and hence to obtain the Fourier transform $G(k)$ of the distribution $\Gamma(\lambda)$. After some further manipulation one finds that

$$\begin{aligned} G_A(k) = \ln M e^{-k^2 s_A^2/2} &[k e^{-a(1-t/T)} \\ &- k \cosh\,k(1-t/T) + a\,\sinh\,k(1-t/T)] \\ &\times [(a^2-k^2)\sinh\,k]^{-1}, \end{aligned} \tag{6.12}$$

$$\begin{aligned} G_C(k) = \ln\,M\,e^{-k^2 s_A^2/2} &[k\,\cosh\,kt/T + a\,\sinh\,kt/T \\ &- (k\,\cosh\,k + a\,\sinh\,k) e^{-a(1-t/T)}] \\ &\times [(a^2-k^2)\sinh\,k]^{-1}, \end{aligned} \tag{6.13}$$

where $a = \ln\,M - k^2 s_A^2/2$ and $s_A = \sigma_A/h$. Clearly $G(0)$ must represent the area under the distribution curve, that is, the total induced charge. It may be confirmed that the Eqns. 6.12 and 6.13 reduce correctly, for $k = 0$, to the Eqns. 6.3a and 6.4a.

6.2.3 Collected charge distributions

The collected positive ion distribution, normalised to q_0, may be expressed as

$$\Gamma_p(\lambda) = \ln\, M \int_{\pi(1-t/T)}^{\pi} \frac{e^{-\lambda/2s_c^2}}{\sqrt{2\pi s_c^2}} M^{-\theta/\pi} d\frac{\theta}{\pi}, \tag{6.14}$$

where

$$s_c^2 = s_A^2(1-\theta/\pi).$$

Thus

$$G_p(k) = \ln\, M[(e^{at/T}-1)/aM]. \tag{6.15}$$

It can be seen that $G_p(0)$ becomes equal to Eqn. 6.4b. For most practical situations $M \gg 1$ and $t \ll T$ so that Γ_p is negligibly small.

The collected electron distribution may be written at once, again normalised to q_0, as

$$\Gamma_e(\lambda) = -\frac{1}{\sqrt{2\pi s_A^2}} e^{-\lambda^2/2s_a^2}. \tag{6.16}$$

6.2.4 Net charge distributions

The net distributions Γ_a and Γ_c observed on the electrodes may now be found from Eqns. 6.12, 6.13 and 6.15, by calculating, numerically, Γ_A, Γ_C and Γ_p, the inverse transforms of G_A, G_C and G_p respectively, and then adding the appropriate induced and collected charge distributions. That is

$$\Gamma(\lambda) = \frac{1}{\pi}\int_0^{\infty} G(k)\cos k\lambda dk, \tag{6.17}$$

and then

$$\Gamma_a = \Gamma_A + \Gamma_e \quad \text{and} \quad \Gamma_c = \Gamma_C + \Gamma_p.$$

6.2.5 Effect of diffusion in drift space

In the present formalism this may be taken into account very easily by multiplying each transform before numerical inversion by the transform of the initial electron distribution. To a good approximation this multiplier is simply $exp(-k^2 s_d^2/2)$ where s_d is the (normalised) standard deviation of the initial distribution. That is

$$s_d = \frac{\sigma_d}{h} = \frac{1}{h}\sqrt{2\frac{D/\mu}{E_d}\, d_0} \tag{6.18}$$

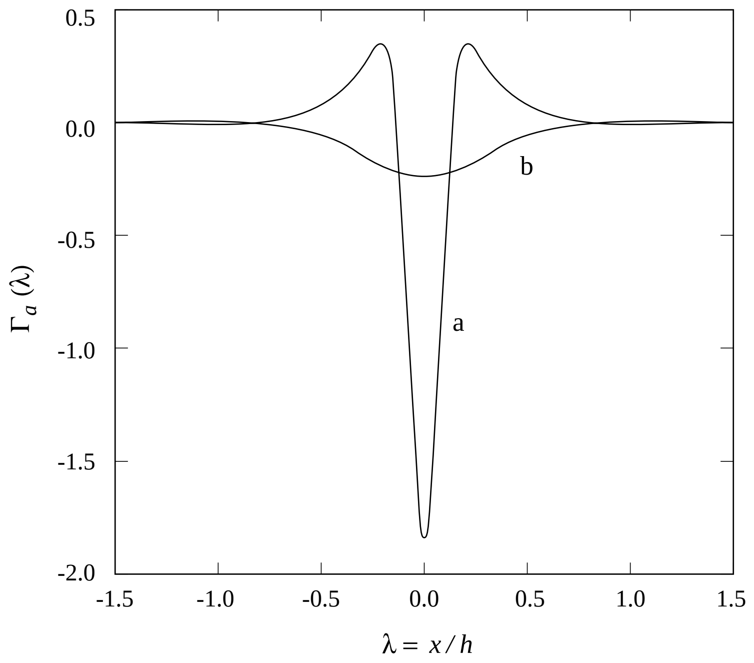

Figure 6.2 Net charge distribution on anode at time $t = 0$. Drift depth (a) 3.0 mm, (b) 7.8 cm. Drift field 270 V/cm. Ar/10%CH$_4$ at 1 atm., gas gain 3.0×10^4.

where D/μ is the electron characteristic energy for drift field E_d and d_0 is the drift distance. D/μ can be estimated quite accurately now for many counting gas mixtures, see for example ref. [12].

For collected electron distribution $\Gamma_e(\lambda)$ it is of course only necessary to replace the variance s_A^2 by the resultant variance $s_A^2 + s_d^2$.

6.3 Example distributions

Examples of anode net distributions (normalised) at time $t = 0$ are shown in Fig. 6.2, for gas gain 3.0×10^4. The two curves correspond to drift depths $d_0 = 3.0mm$ and 7.8cm in P10 gas at 1 atm with drift field $E_d = 270\,\text{V/cm}$. For the present illustrative calculations the value employed for s_A was 0.053, an approximate figure derived from the direct measurement of Peisert [6] under comparable conditions. The normalised FWHM values for these two distributions are 0.16 and 0.65, in quite acceptable agreement with experimental values obtained under similar conditions by Peisert and Sauli [8] of 0.20 and 0.53 respectively.

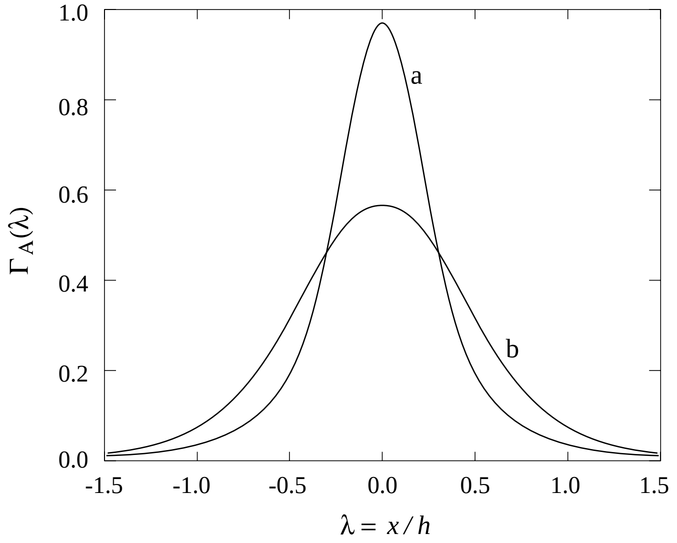

Figure 6.3 Induced charge distributions on anode at time $t/T = 0.2$. Drift depth (a) 3.0 mm, (b) 7.8 cm. Drift field 270 V/cm. Ar/10%CH_4 at 1 atm., gas gain 3.0×10^4.

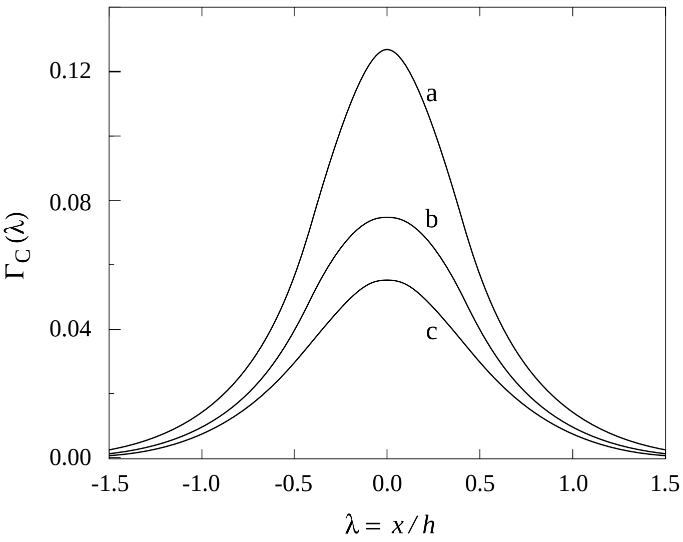

Figure 6.4 Induced charge distribution on cathode at time $t = 0$. (a) $M = 10^3$, FWHM = 0.970, (b) $M = 3.0\times10^4$, FWHM = 1.09, (c) $M = 10^6$, FWHM = 1.13.

Fig. 6.3 shows anode induced charge distributions at time $t/T = 0.2$ for the same two drift cases. The two distributions, with FWHM = 0.57 and 1.1, would be very roughly similar in shape, but of course not in magnitude, to those observed on a pick-up electrode situated $\approx h/4$ below an anode transparent to the field of the positive ions. This very crudely models the actual situation realised in the work of Peisert and Sauli [8] who observed widths of 0.50 and 0.80 respectively.

Fig. 6.4 illustrates the (very small) dependence of the width of the induced charge distributions on gas gain. Conditions are as in the previous examples, with drift depth $d_0 = 3.00$mm, and s_A has been assumed constant.

6.4 Discussion

Lack of knowledge of σ_A represents the largest uncertainty in the calculations of net anode distributions. Raether [3] has given some experimental figures relating to pure gases but there appears to be only one direct measurement, that of Peisert [6], for a common counting gas mixture. Further experimental data is required in this area. It may also be possible to obtain quite accurate estimates of σ_A theoretically, see for example ref. [13]. The induced charge distributions are naturally somewhat less sensitive to the choice of , σ_A.

The actual calculations Eqn. 6.17, the Fourier inversion of Eqns. 6.12, 6.13 and 6.15 are, with standard library routines now available, very simple.

If the initial electron swarm crosses the cathode with a time duration comparable with signal processing time constants then the signal charge functions must be obtained by convolution of the appropriate distribution with the initial current waveform $i(t)$. If this waveform is essentially due to diffusion in the drift region then it may be approximated by

$$i(t) = \frac{q_0/M}{\sqrt{2\pi\sigma_t^2}} e^{-t^2/2\sigma_t^2}. \tag{6.19}$$

with $\sigma_t = \sigma_L/w$, where w is the drift velocity in the drift region and σ_L is given by Eqn. 6.18 with the lateral diffusion coefficient D replaced by the longitudinal coefficient D_L (see for example, ref. [12]).

References

1. K.J. Schmidt, Z. Phys. 193 (1954) 251.
2. J.E. Draper, Nucl. Instr. & Meth. 30 (1964) 148.
3. H. Raether, Electron Avalanches and Breakdown in Gases (Butterworth, London, 1964).

4. J.W. Stumpel, P.W. Sanford and H.F. Goddard, J. Phys. E. (Sci. Instr.) 6 (1973) 397.
5. J.A. Bleeker, H. Huizenga, A.J.F. den Boggende and A.C. Brinkman, IEEE Trans. Nucl. Sci. NS-27 (1980) 176.
6. A. Peisert, Nucl. Instr. & Meth. 217 (1983) 229.
7. J. Hendrix, IEEE Trans. Nucl. Sci. NS-31 (1984) 281.
8. A. Peisert & F. Sauli, Nucl. Instr. & Meth. A247 (1986) 453.
9. D.J. Harrach & H.J. Specht. Nucl. Instr. & Meth. 164 (1979) 477.
10. R. Bellazzini, C. Betti, A. Brez, E. Carboni, M.M. Massai & M.R. Torquati, Nucl. Instr. & Meth. A247 (1986) 445.
11. I.S. Gradstheyn & I.M. Ryzhik, Table of Integrals, Series and Products (Academic Press, Orlando, 1980).
12. G.W. Fraser & E. Mathieson, Nucl. Instr. & Meth. A247 (1986) 544.
13. T. Ohmori, K. Kitamori, M. Shimozuma & H. Tagashira, J. Phys. D (Appl. Phys.) 19 (1986) 437.
14. E. Mathieson & G.C. Smith, Nucl. Instr. & Meth. A273 (1988) 518.

Chapter 7.

COAXIAL GEOMETRY II. Cathode charge distributions

7.1 Introduction

In Chapter 2 simple formulae were derived to describe the time development of the net anode, and cathode, charges. In some applications it becomes necessary to determine the spatial distribution of the induced cathode charge. For example, information may be obtained on the physical structure of streamers by examining experimentally the relative charges induced on the segmented cathodes of a coaxial chamber [1]. Further information may possibly be obtained on the streamer structure by comparing experimental current waveforms with the predictions of various, theoretical models (see Section 7.5 below).

Although involving simple coaxial geometry only the calculation of induced charge distribution is nevertheless relatively complicated.

7.2 Basic theory

The following brief theoretical notes are intended only as a reminder and to introduce some terminology. For a correct mathematical introduction the reader should consult one of the many texts on functions of a complex variable and conformal mapping (see, for example, ref [2]; see also Appendix 1).

If an analytic function $W(z)$ of the complex variable $z = x + iy$ can be expressed in the form

$$W(z) = P(x, y) + iQ(x, y) \tag{7.1}$$

where $P(x, y)$ and $Q(x, y)$ are real functions of x and y, then it follows at once that the conjugate functions P and Q are harmonic functions, that is they are solutions of Laplace's equation.

$$\frac{\partial^2 P}{\partial x^2} + \frac{\partial^2 P}{\partial y^2} = 0 \quad \text{and} \quad \frac{\partial^2 Q}{\partial x^2} + \frac{\partial^2 Q}{\partial y^2} = 0$$

It also follows that the families of curves $P =$ constant and $Q =$ constant intersect orthogonally. Thus $P =$ constant may represent equipotentials and $Q =$ constant the corresponding field lines in a particular problem (or vice versa).

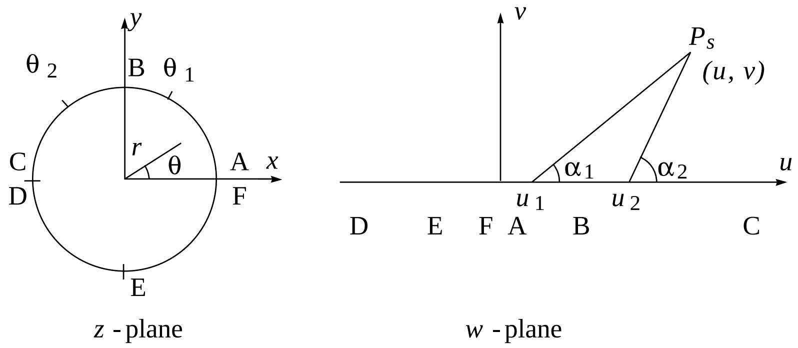

Figure 7.1

It may further be shown that a harmonic function remains harmonic under conformal transformation, ref [2], p.242. Thus one problem may sometimes be transformed into another with a well-known or simple solution. This strategy will be employed below.

7.3 Azimuthal distribution of cathode charge

7.3.1 Approximate formula

Consider the transformation, Fig. 7.1,

$$w = i\frac{1 - z/r_c}{1 + z/r_c} \tag{7.2}$$

where $w = u + iv$. After some manipulation Eqn. 7.2 may be re-written

$$u + iv = \frac{2(r/r_c)\sin\theta + i(1 - (r/r_c)^2)}{1 + 2(r/r_c)\cos\theta + (r/r_c)^2} \tag{7.3}$$

where $r = (x^2 + y^2)^{1/2}$ and $\theta = \tan^{-1}(y/x)$. Thus the circle $r = r_c$ in the z-plane transforms to the u-axis in the w-plane. On this axis $u = \tan\theta/2$.

It is a standard result of electrostatic theory, see Appendix 2, that the potential $P_s(u, v)$ due to a strip on the u-axis at unit potential, the remainder of the plane being grounded, is given by

$$P_s(u, v) = (\alpha_2 - \alpha_1)/\pi \tag{7.4}$$

where, as shown in Fig. 7.1, α_1 and α_2 are the angles subtended by the point (u, v) to the strip edges at u_1 and u_2 respectively. From Fig. 7.1

$$\tan(\alpha_2 - \alpha_1) = \frac{u(u_2 - u_1)}{v^2 + (u - u_2)(u - u_1)} \tag{7.5}$$

The axis orientation may be chosen, without loss of generality, so that the point at which P_s is calculated is on the x-axis, $\theta = 0$. Then, from Eqn. 7.3,

$$u = 0 \tag{7.6a}$$

$$v = (1 - r/r_c)/(1 + r/r_c) \tag{7.6b}$$

and

$$\tan(\alpha_2 - \alpha_1) = \frac{v(\tan\theta_2/2 - \tan\theta_1/2)}{v^2 + \tan\theta_2/2 \ \tan\theta_1/2} \tag{7.7}$$

Now if an anode wire is present there must be an induced charge on the wire, producing in the chamber an additional potential distribution P_w. Provided $r_a \ll r_c$ this distribution will be symmetrical and of the form Eqn. 2.4.

$$P_w = P_a[1 - C \ \ln(r/r_a)^2] \tag{7.8}$$

where $C = 1/\ln(r_c/r_a)^2$. P_a is determined by the condition that the surface of the anode wire must be at zero potential, $P_s + P_w = 0$ at $r = r_a$. Now since $r_a \ll r_c$, near the wire surface $v = 1$ and $(\alpha_2 - \alpha_1) = (\theta_2 - \theta_1)/2$. Thus

$$P_a = -(\theta_2 - \theta_1)/2\pi \tag{7.9}$$

Hence the potential function due to the cathode segment between θ_1 and θ_2 being at unit potential, the remainder of the cathode being grounded, is

$$P = \frac{\alpha_2 - \alpha_1}{\pi} - \frac{\theta_2 - \theta_1}{2\pi}[1 - C\ln(r/r_c)^2] \tag{7.10}$$

where $\tan(\alpha_2 - \alpha_1)$ is given by Eqns. 7.7 and 7.6.

The charge $-q$ induced on that segment by a point charge q_0 at radius r on the x-axis is therefore given by, from Section 1.1,

$$q = q_0 P \tag{7.11}$$

It may be more convenient to re-express the above result in terms of a differential induced charge distribution. Let $-\rho(\theta)d\theta$ be the charge induced on the cathode surface between θ and $\theta + d\theta$. That is, placing $\theta_2 = \theta$

$$\rho(\theta) = q_0 \frac{\partial P}{\partial \theta} \tag{7.12}$$

After some manipulation, first placing $\theta_2 = \theta$ and $\theta_1 = 0$ in Eqn. 7.10, it is found that

$$\rho(\theta) = \frac{q_0}{2\pi}\left\{\frac{v}{v^2\cos^2\theta/2 + \sin^2\theta/2} - 1 + C\ln\left(\frac{r}{r_a}\right)^2\right\} \tag{7.13}$$

where $v = (1 - r/r_c)/(1 + r/r_c)$.

The result Eqn. 7.13 may be confirmed by evaluating the total induced cathode charge by integrating $\rho(\theta)$ with respect to θ from 0 to 2π. With the aid of the integral, ref. [3], p.325.

$$\int \frac{a d\varphi}{a^2 \cos^2 \varphi + \sin^2 \varphi} = \tan^{-1} \frac{\tan \varphi}{a}$$

it is soon found that

$$\int_0^{2\pi} \rho(\theta) d\theta = q_0 C \ln(r/r_a)^2 \tag{7.14}$$

in agreement with Eqn. 2.7.

In proportional chamber work generally it is sensible, in order to remove gross time dependence, to normalise to the net anode signal (see for example Chap.5). That is, we define a normalised distribution function $\Gamma(\theta) = \rho(\theta)/|q_a|$ where, from Eqn. 2.6, $q_a = -q_0\ C \ln(r/r_a)^2$. Clearly

$$\int_0^{2\pi} \Gamma(\theta)\, d\theta = 1. \tag{7.15}$$

7.3.2 Exact formula

In deriving the potential function Eqn. 7.10 it was implicitly assumed that the induced anode charge can be replaced by a line charge coincident with the system axis. This is not quite correct, the line charge being slightly displaced towards the inducing cathode sector. As r becomes large compared with r_a the error introduced by this assumption becomes rapidly negligible.

Erskine [4] has derived an exact formula for the potential function. Corresponding to Eqn. 7.10, with $\theta_1 = 0$ and $\theta_2 = \theta$, the exact formula is

$$P = \frac{1}{\pi} \sum_1^\infty \frac{1}{n} \left(\frac{r}{r_c}\right)^n \frac{1 - (r_a/r)^{2n}}{1 - (r_a/r_c)^{2n}} \sin n\theta + \frac{\theta}{2\pi} C \ln \left(\frac{r}{r_a}\right)^2 \tag{7.16}$$

Recent numerical calculations [5] have demonstrated that, for $r/r_a > 3.3$, Eqns. 7.10 and 7.16 differ by less than 1%.

7.4 Axial and azimuthal distribution of cathode charge

In order to find the complete distribution of cathode induced charge in a coaxial counter, $-\sigma(\theta, z)$, the surface field method rather than the reciprocity method must be employed. That is, if $E_n(\theta, z)$ is the field at the cathode surface then

$$\sigma(\theta, z) = \epsilon_0 E_n(\theta, z) \tag{7.17}$$

Cylindrical coordinates are employed in this section, with the anode wire along the z-axis.

An exact expression can be found for E_n, without any restriction on the value of r_a/r_c. The analysis developed below parallels that employed by Smythe [6] in a similar problem.

Suppose the inducing point charge q_0 to be situated at radius r_0, azimuthal angle $\theta = 0$ and at axial position $z = 0$. Then we wish to find, initially, the potential function $P(r, \theta, z)$ due to this situation.

Define a function $F_{mk}(\mu_{mk} r)$ as follows

$$F_{mk} = J_m(\mu_{mk} r) - Y_m(\mu_{mk} r) J_m(\mu_{mk} r_a)/Y_m(\mu_{mk} r_a) \tag{7.18}$$

where J_m, Y_m are Bessel functions of the first, second kinds respectively [7]. It is seen that $F_{mk}(\mu_{mk} r_a) = 0$. The coefficients μ_{mk} are determined by the condition

$$F_{mk}(\mu_{mk} r_c) = 0 \tag{7.19}$$

A suitable potential function can now be written

$$P(r, \theta, z) = \frac{q_0}{2\pi\epsilon_0} \sum_{k=1}^{\infty} \sum_{m=0}^{\infty} A_{mk} F_{mk}(\mu r) e^{-\mu|z|} \cos m\theta \tag{7.20}$$

where, for convenience, μ has been written in place of μ_{mk}.

In order to evaluate the coefficients A_{mk} we proceed as follows. Differentiate with respect to z, and set $z = 0$. Then multiply both sides of the resulting equation by $r F_{nl}(\mu_{nl} r) \cos n\theta$ and integrate from 0 to 2π with respect to θ and from r_a to r_c with respect to r.

The RHS integral over θ vanishes for all terms unless $n = m$. A factor $\delta'_m = 2\pi$ occurs if $m = 0$ or $\delta'_m = \pi$ if $m > 0$. Further, since $F_{mk}(\mu r_a) = F_{mk}(\mu r_c) = F_{ml}(\mu r_a) = F_{ml}(\mu r_c) = 0$, it can be shown that all terms vanish unless $l = k$. Thus we obtain

$$\int_{r_a}^{r_c} \int_0^{2\pi} \left(\frac{\partial P}{\partial z}\right)_0 F_{mk}(\mu r) r dr\theta = -\frac{q_0}{2\pi\epsilon_0} A_{mk} \mu \delta'_m \int_{r_a}^{r_c} r F_{mk}^2(\mu r) dr \tag{7.21}$$

Note that $\cos m\theta$ does not appear in the LHS since $(\partial P/\partial z)_0$ is zero for all positions in the plane $z = 0$ except at the point charge itself, where $\theta = 0$ and hence $\cos m\theta = 1$. Thus in evaluating the LHS of Eqn. 7.21, $F_{mk}(\mu r)$ may be replaced by $F_{mk}(\mu r_0)$ and taken outside the integral. The integral itself then becomes simply the flux, in one direction, of the normal component of field over the plane $z = 0$ and, by Gauss's theorem, this is equal to $q_0/2\epsilon_0$. Thus the LHS of Eqn. 7.21 becomes $-F_{mk}(\mu r_0)q_0/2\epsilon_0$.

Evaluation of the RHS requires the use of special properties of the Bessel functions. It is a property of any solution R_n of Bessel's equation that (ref. [6], pg.176)

$$\int_0^a vR_n^2(v)dv = \frac{1}{2}|v^2\left(\frac{dR_n}{dv}\right)^2 + (v^2 - n^2)R_n^2|_0^a$$

If $R_n(a) = R_n(b) = 0$, as in the present application, then

$$\int_a^b vR_n^2(v)dv = \frac{1}{2}|v^2 R_n'^2|_a^b$$

where $R_n'(v) = dR_n/dv$. Employing this result, the RHS of Eqn. 7.21 may be written

$$RHS = -\frac{q_o}{4\pi\epsilon_0}A_{mk}\delta_m'\mu|(rF_{mk}'(\mu r))^2|_{r_a}^{r_b}$$

Hence Eqn. 7.21 leads to an expression for A_{mk}

$$A_{mk} = (2 - \delta_m)\frac{F_{mk}(\mu r_0)}{\mu|(rF_{mk}'(\mu r))^2|_{r_a}^{r_c}} \tag{7.22}$$

where $\delta_m = 1$ for $m = 0$ and $\delta_m = 0$ for $m > 0$. In evaluating these coefficients it should be noted that, from the recurrence relationships [6,7], for $r = r_a$ or $r = r_c$,

$$F_{mk}'(\mu r) = -[J_{m+1}(\mu r) - Y_{m+1}(\mu r)J_m(\mu r_a)/Y_m(\mu r_a)] \tag{7.23}$$

The induced cathode charge per unit area $-\sigma(\theta, z)$ is given by

$$\sigma(\theta, z) = -\epsilon_0\left(\frac{\partial P}{\partial r}\right)_{r_c}$$

From Eqns. 7.20 and 7.22 this expression may be written

$$\sigma(\theta, z) = q_0\sum_{k=1}^{\infty}\sum_{m=0}^{\infty}C_{mk}e^{-\mu|z|}\cos m\theta \tag{7.24}$$

where

$$C_{mk} = -\frac{\mu}{2\pi} A_{mk} F'_{mk}(\mu r_c) \tag{7.25}$$

and $\mu = \mu_{mk}$ is determined by Eqn. 7.19.

For comparison with any experimental situation Eqn. 7.24 would be integrated between particular limits θ_1 and θ_2, and between z_1 and z_2, say.

A partial check on the correctness of numerical calculations may be obtained by evaluation of total induced charge

$$q_c = q_0 \sum_{k=1}^{\infty} A_{ok} F'_{ok}(\mu r_c) \tag{7.26}$$

where $\mu = \mu_{ok}$. This expression must of course be numerically equal to $q_0\, C \ln(r_0/r_a)^2$, Eqn. 2.7.

7.5 Current waveforms from radial streamers

7.5.1 Introduction

It is instructive to complete this chapter by considering briefly a simple model that may be of assistance towards understanding certain aspects of streamer operation in coaxial chambers. At the University of Coimbra, Portugal a group led by Policarpo [8] is currently making detailed experimental measurements of the anode, and cathode sector, waveforms due to streamers. These waveforms have very fast rise-times, mainly determined by signal processing, and short overall duration, $\sim 100\,\text{ns}$.

The detailed shape of the current waveform must depend upon many factors. Most important among these are the distribution of charge along the streamer length, the streamer propagation velocity, the physical shape of the streamer and the electron velocity within the streamer. This is a complex situation which would clearly be difficult to explore in detail. However by assuming a strictly radial streamer, and by making the highly simplifying assumptions of constant electron velocity and constant streamer propagation velocity, it becomes possible to predict anode and cathode sectors current waveforms for various trial distribution functions. This very simple model may thus represent a departure point for more sophisticated approaches.

7.5.2 Anode current waveforms

The following analysis may be understood with the aid of Fig. 7.2.

Suppose the streamer head is at radius r_s advancing with constant velocity v_s. Then there must be a radius r_1 within which there is no electron contribution to the present current (the electrons having already been collected). That is,

$$(r_s - r_1)/v_s = (r_1 - r_a)/v_e$$

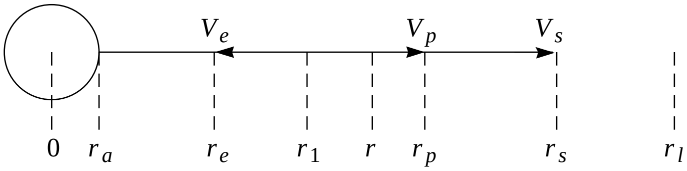

Figure 7.2

where v_e is the (constant) electron velocity. Thus

$$r_1(1/v_s + 1/v_e) = r_s/v_s + r_a/v_e \tag{7.27}$$

The electrons produced at radius r will have moved to r_e where

$$(r_s - r)/v_s = (r - r_e)/v_e$$

or

$$r_e/v_e = r(1/v_s + 1/v_e) - r_s/v_s \tag{7.28}$$

In the present model we must envisage r_s to increase continually but the ionisation density $\rho(r)$ to reduce to zero at, say, r_l. The streamer length is $(r_l - r_a)$. Time thus enters the model through the equation

$$(r_s - r_a) = v_s t \tag{7.29}$$

and the streamer propagation stops at time $t_l = (r_l - r_a)/v_s$.

The current does not stop then of course but continues to be carried by the electrons and, to a much smaller extent, by the ions.

The electron contribution to the anode current, $i_e(t)$, may now be obtained as follows. The electron charge $-\rho(r)dr$ created at radius r has now travelled to r_e, given by Eqn. 7.28. Thus, according to Eqns. 1.5b and 2.5, the present contribution to anode current is

$$di_e(t) = -\rho(r)dr\frac{d}{dt}[1 - C\ln(r_e/r_a)^2] \tag{7.30a}$$

$$= -2Cv_e\frac{\rho(r)dr}{r_e} \tag{7.30b}$$

where $-dr_e/dt = v_e$, the constant electron velocity.
If $t < t_l$

$$i_e(t) = -2Cv_e\int_{r_1}^{r_s}\frac{\rho(r)dr}{r_e} \tag{7.31}$$

Here r_e is a function of r, though Eqn. 7.28, and of course r_1 and r_2 are functions of time t though Eqns. 7.27 and 7.29.

If $t > t_l$ and $t \leq t_e = (r_l - r_a)/v_e$ then the streamer has stopped but electrons, and ions, continue to flow. The upper limit of the integral in Eqn. 7.31 must be changed from r_s to r_l.

$$i_e(t) = -2Cv_e \int_{r_1}^{r_\ell} \frac{\rho(r)dr}{r_e} \tag{7.32}$$

If $t > t_l$ and $t > t_e$ then electron flow has ceased, $i_e(t) = 0$, and only a very small ion current remains.

The positive ion contribution to the anode current, $i_p(t)$, is negligibly small and could reasonably be omitted altogether. However it is very simple to include a contribution, on the assumption of constant ion mobility in the applied field. In fact the heavy space charge already existing should really be taken into account but this problem has so far proved intractable. Thus, ignoring the space charge, the ions move from r to r_p in a time $(r_s - r)/v_s$ where according to Eqn. 2.11,

$$(r_p^2 - r^2)/r_a^2 = 1 + (r_s - r)/v_s t_0 \tag{7.33}$$

Here t_0 is the characteristic time defined in Eqn. 2.10. Thus

$$(r_p/r_a)^2 = (r/r_a)^2 + (r_s - r)/v_s t_0 \tag{7.34}$$

The contribution $di_p(t)$ is given by a similar expression to Eqn. 7.30, with a positive sign, but in this case the ion velocity dr_p/dt is not constant. From Eqns. 2.8 and 2.10 of Chapter 2

$$\frac{dr_p}{dt} = \frac{r_a^2}{2t_o r_p} \tag{7.35}$$

Thus

$$di_p(t) = -Cv_0 r_a \frac{\rho(r)dr}{r_p^2} \tag{7.36}$$

where, for convenience, $v_0 = r_a/t_0$. Then

$$i_p(t) = -Cv_0 r_a \int_{r_a}^{r_u} \frac{\rho(r)dr}{r_p^2} \tag{7.37}$$

The upper limit r_u of the integral in Eqn. 7.37 is r_s for $t < t_l$ and r_l for $t \geq t_l$.

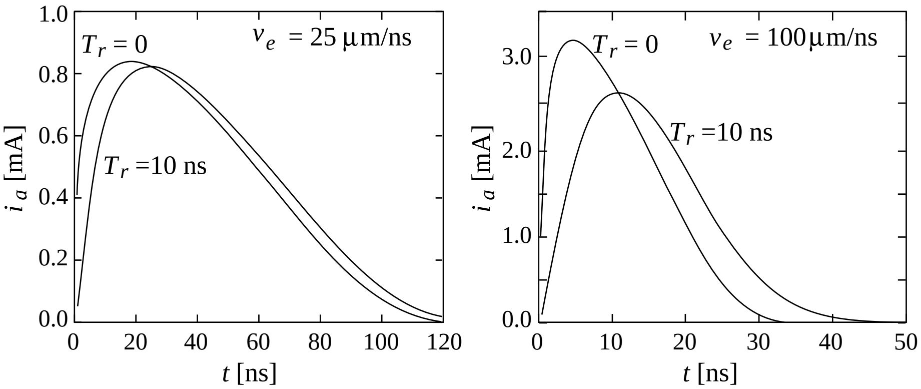

Figure 7.3 Anode current waveforms due to a radial streamer with Gallimberti [8] charge distribution. The streamer length is 3.0 mm and the total charge is 97 pC. A constant propagation velocity of 1000 μm/ns has been assumed. The results for two (constant) electron velocities are shown, before and after signal processing with 10–90% rise-time of 10 ns.
Chamber parameters are: anode radius 50 μm, cathode radius 12 mm, anode voltage 5 kV.

Thus, finally, the anode current waveform is given by

$$i_a(t) = i_e(t) + i_p(t) \tag{7.38}$$

As mentioned above, in realistic calculations the positive ion contribution proves to be negligibly small compared with the electron contribution.

The rise-time of the current waveform is very short. It is therefore essential, if realistic comparisons are to be made with experiment, to take into account signal processing integration. This may be accomplished by convolution of the calculated current waveform with the appropriate impulse response of the system. Fig. 7.3 shows an example of calculated anode waveforms, before and after signal processing. The charge density $\rho(r)$ employed for these calculations was derived by the Coimbra group [8] from a theoretical treatment of discharge development by Gallimberti [9]. The assumed velocities v_e and v_s, and the chamber parameters, are indicated with the figure.

7.5.3 Cathode sector current waveform

The current waveform from a sector of the cathode can also be calculated using the same model as in the previous section. However in this case the current is derived from the expression for induced charge derived in Section 7.3.1.

For a streamer developing along the $\theta = 0$ axis, Fig. 7.1, the electron and ion contributions to the current of a cathode sector between θ_1 and θ_2 are given by, respectively,

$$i_e = v_e \int \left(\frac{dP}{dr}\right)_{r_e} \rho(r)\, dr \tag{7.39}$$

$$i_p = \frac{v_0 r_a}{2} \int \left(\frac{dP}{dr}\right)_{r_p} \frac{\rho(r)}{r_p} dr \tag{7.40}$$

where $P(r, \theta_1, \theta_2)$ is given by Eqn. 7.10. The differentials must be evaluated at the appropriate radii as indicated. The limits of the integrals are the same as in the previous section. The expression for dP/dr is rather clumsy, but straightforward.

$$\frac{dP}{dr} = -\frac{2a(b - v^2)}{\pi[(v^2 + b)^2 + v^2 a^2]} \frac{1}{r_c(1 + r/r_c)^2} + \frac{\theta_2 - \theta_1}{\pi} \frac{C}{r} \tag{7.41}$$

where

$$\begin{aligned} a &= \tan\theta_2/2 - \tan\theta_1/2 \\ b &= \tan\theta_2/2 . \tan\theta_1/2 \\ v &= (1 - r/r_c)/(1 + r/r_c) \end{aligned}$$

References

1. E.P. de Lima, R. Ferreira Marques, J.M. Garabatos, A.J.P.L. Policarpo & C.M. Rulea, Port. J. Phys. 17(1986)21.
   E.P. de Lima, J.L. Pinto da Cunha, R. Ferreire-Marques & A.J.P.L. Policarpo, Nucl. Instr. & Meth. A267 (1988) 93.
2. M.R. Spiegel, Theory and Problems of Complex Variables, Schaum McGraw-Hill, New York, 1964.
3. B.O. Pierce, A Short Table of Integrals, Ginn & Co., New York, 1956.
4. G.A. Erskine, (quoted by E.P. de Lima et al. Nucl. Instr. & Meth. A267 (1988) 93.)
5. E.P. de Lima, Ph.D. Thesis, Univ. of Coimbra, Portugal, 1987.
6. W.R. Smythe, Static and Dynamic Electricity, McGraw-Hill, New York, 1950.

7. M. Abramovitz & I.A. Stegun, Handbook of Mathematical Functions, Dover, New York, 1965.
8. F.A.F. de Fraga, R. Ferreira Marques, J.C.L. de Carvalho & A.J.P.L. Policarpo, Nucl. Instr. & Meth. A279 (1989) 339.
   F.A.F. de Fraga (private communication)
9. I. Gallimberti, J. de Phys. 40 (1979) C7–194.

Appendix 1.

Weber approximation for potential function in MWPC

1.1 Mathematical preliminaries

The theoretical methods employed in this, and the following two, appendices will be described in a physicist's rather than a mathematician's terms. The reader to whom rigorous treatment has an essential priority is advised to consult first one of the many excellent texts on functions of a complex variable. Particularly recommended, for the treatment of relevant topics, and for enjoyable further education, is the text by Spiegel [1]. The well-known, standard texts, on electricity, for example ref. [2], and on mathematical physics [3,4], are of course also helpful.

Consider an analytic function $W(z)$ of the complex variable $z = x+iy$ that can be expressed in the form

$$W(z) = P(x,y) + iQ(x,y)$$

where the conjugate functions P and Q are real functions of x, y. Differentiating partially with respect to x and y we have

$$\frac{\partial P}{\partial x} + i\frac{\partial Q}{\partial x} = \frac{dW}{dz}$$
$$\frac{\partial P}{\partial y} + i\frac{\partial Q}{\partial y} = i\frac{dW}{dz}$$

Thus

$$\frac{\partial P}{\partial x} + i\frac{\partial Q}{\partial x} = \frac{\partial Q}{\partial y} - i\frac{\partial P}{\partial y}$$

Hence

$$\frac{\partial P}{\partial x} = \frac{\partial Q}{\partial y} \quad \text{and} \quad \frac{\partial P}{\partial y} = -\frac{\partial Q}{\partial x}$$

These expressions are known as the Cauchy-Riemann equations. It follows from these equations that

$$\frac{\partial^2 P}{\partial x^2} + \frac{\partial^2 P}{\partial y^2} = 0 \quad \text{and} \quad \frac{\partial^2 Q}{\partial x^2} + \frac{\partial^2 Q}{\partial y^2} = 0$$

Thus conjugate functions are harmonic functions (i.e. solutions of Laplace's equations) and possible candidates for our attention.

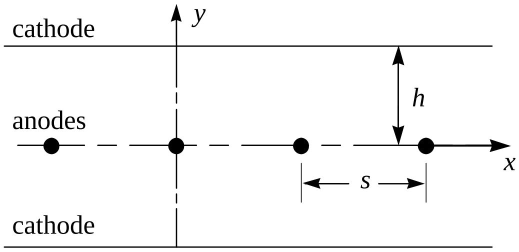

Figure A1.1

Consider the curve $P(x, y)$ = constant. The slope of this curve at (x, y) is

$$\left(\frac{dy}{dx}\right)_P = -\frac{\partial P}{\partial x} \Big/ \frac{\partial P}{\partial y}$$

The slope of the curve $Q(x, y)$ = constant at the same point is

$$\left(\frac{dy}{dx}\right)_Q = -\frac{\partial Q}{\partial x} \Big/ \frac{\partial Q}{\partial y}$$

Hence, from the Cauchy-Riemmann equations,

$$\left(\frac{dy}{dx}\right)_P \left(\frac{dy}{dx}\right)_Q = -1$$

Thus the two families of curves, P = constant and Q = constant, intersect orthogonally. The first could represent the equipotentials in a particular system and the second the corresponding field lines (or vice versa).

An important property of harmonic functions is that they remain harmonic under a conformal transformation [1, p.242]. Thus it may occur in a particular problem that the boundaries in the z-plane, may be mapped into others, in the w-plane, for which a simple solution may be obtained. This technique will be used in Appendices 2 and 3.

1.2 Symmetrical multiwire chamber

1.2.1 Anode at unit potential

A symmetrical multiwire chamber is shown schematically in Fig.A1.1, the anode wires being normal to the $x - y$ plane. The anode, cathode spacing is h and the (constant) anode wire pitch is s. It is assumed, as in all the wire chamber treatments in this monograph, that the wire radius r_a is very small compared with s.

The assumption which characterises this present formulation, one of the problems treated by Weber [5], is that the ratio h/s is such that $\cosh(2\pi h/s) \gg 1$.

Consider the complex potential function $W(z)$ given by

$$W(z) = -K \ln\{\sin(\pi z/s)\} - i\, E_0 z + V_0 \tag{A1.1}$$

where K, E_0 and V_0 are constants. Then $W(z)$ can be expressed as

$$W(z) = P(x, y) + iQ(x, y) \tag{A1.2}$$

where, after some manipulation, it is found that

$$P(x, y) = -K \ln\{(\cosh 2\pi y/s - \cos 2\pi x/s)/2\}^{\frac{1}{2}} + E_0 y + V_0 \tag{A1.3}$$

and

$$Q(x, y) = -K\beta - E_0 x \tag{A1.4}$$

where

$$\tan\beta = \tanh \pi y/s/ \tan \pi x/s \tag{A1.5}$$

If we examine the value of the curly bracket in Eqn. A1.3 in the close proximity to an anode wire, that is when $y/s \to 0$ and $x'/s \to 0$ where $x' = x - ns$, then it is found that

$$\{(\cosh 2\pi y/s - \cos 2\pi x/s)/2\}^{\frac{1}{2}} \to \pi r/s \tag{A1.6}$$

where

$$r = (x'^2 + y^2)^{1/2}$$

Now examine the value of the curly bracket in Eqn. A1.3 when $\cosh 2\pi y/s \gg 1$. Under these conditions

$$\ln\{(\cosh 2\pi y/s - \cos 2\pi x/s)\}^{\frac{1}{2}} = \pi|y|/s - \ln 2 \tag{A1.7}$$

It is convenient now, and for later work, to define an effective cathode radius r_c by means of the expression

$$r_c = (s/2\pi)e^{\pi h/s} \tag{A1.8}$$

Then

$$\ln\{(\cosh 2\pi y/s - \cos 2\pi x/s)/2\}^{\frac{1}{2}} = \ln \pi r_c/s - (1 - |y|/h)\pi h/s \tag{A1.9}$$

We can now determine the constants K, E_0 and V_0. For, if the anode is at unit potential and the two cathodes are grounded, then,

at $y = h$, $0 = -K \ln \pi r_c/s + E_0 h + V_0$
at $r = r_a$, $1 = -K \ln \pi r_a/s + V_0$
and at $y = -h$, $0 = -K \ln \pi r_c/s - E_0 h + V_0$

From these simultaneous equations it is seen that

$$\begin{aligned} E_0 &= 0 \\ V_0 &= K \ln \pi r_c/s \\ K &= 1/\ln(r_c/r_a) \end{aligned}$$

It is useful to define a dimensionless quantity C, as in Eqn. 2.2,

$$C = 1/\ln(r_c/r_a)^2 \qquad (A1.10)$$

Thus

$$K = 2C.$$

Then, after some algebraic manipulation, the potential function $P(x,y)$, Eqn. A1.3, may be finally written

$$P(x,y) = 1 - C \ln \frac{\{2(\cosh 2\pi y/s - \cos 2\pi x/s)\}}{(2\pi r_a/s)^2} \qquad (A1.11)$$

It is clear, from Eqn. A1.6, that close to an anode wire this potential function reduces, as expected, to the simple coaxial form

$$P(r) = 1 - C \ln(r/r_a)^2$$

In the body of the chamber, well away from the anode wire plane, where $\cosh 2\pi y/s \gg 1$, then using Eqn. A1.7 the potential function reduces to

$$P(y) = \frac{2\pi Ch}{s}\left(1 - \frac{|y|}{h}\right) \qquad (A1.12)$$

The flux function Eqn. A1.4 may be written

$$Q(x,y) = -2C \tan^{-1}\left(\frac{\tanh \pi y/s}{\tan \pi x/s}\right) \qquad (A1.13)$$

A field line is defined by the expression $Q =$ constant. At very small values of y/s and $(x' - ns)/s$, near an anode wire, $y/x' = \alpha$ where α is the angle at which the field line meets the anode wire surface. Thus the field lines are described by the family of curves

$$\tanh \pi y/s = \tan \alpha . \tan \pi x/s \qquad (A1.14)$$

1.2.2 Cathode at unit potential

If the upper cathode in Fig. A1.1 is at unit potential and the anode and lower cathode are grounded then the constants in Eqn. A1.3 are determined by the three equations,

at $y = \; h$, $1 = -K \ln \pi r_c/s + E_0 h + V_0$
at $r = \; r_a$, $0 = -K \ln \pi r_a/s + V_0$
and at $y = -h$, $0 = -K \ln \pi r_c/s - E_0 h + V_0$

From these conditions, and using Eqn. A1.10 again, we find

$$E_0 = 1/2h$$
$$V_0 = -C \ln \pi r_a/s$$
$$K = -C$$

Thus in this case the potential function $P(x, y)$ becomes

$$P(x, y) = \frac{C}{2} \ln \frac{\{2(\cosh 2\pi y/s - \cos 2\pi x/s)\}}{(2\pi r_a/s)^2} + \frac{y}{2h} \qquad (A1.15)$$

In the region close to the wire this function reduces to, with the aid of Eqn. A1.6,

$$P(r) = \frac{C}{2} \ln \left(\frac{r}{r_a} \right)^2 \qquad (A1.16)$$

In the body of the chamber, where $\cosh 2\pi y/s \gg 1$, then using Eqn. A1.7,

$$P(y) = \frac{1}{2}\left(1 + \frac{y}{h}\right) - \frac{\pi C h}{s}\left(1 - \frac{|y|}{h}\right) \qquad (A1.17)$$

The field in the body of the chamber is given by

$$E(y) = -\frac{1}{2h}\left(1 \pm \frac{2\pi C h}{s}\right) \qquad (A1.18)$$

where the plus, minus signs refer to the upper, lower regions respectively. Clearly the magnitude of the field is much smaller in the lower region because of the shielding of the anode plane.

The flux function Eqn. A1.4 with the upper cathode at unit potential now becomes

$$Q(x,y) = C \tan^{-1}\left(\frac{\tanh \pi y/s}{\tan \pi x/s}\right) - \frac{x}{2h} \tag{A1.19}$$

and the field lines are therefore defined by the equation

$$\tanh \pi y/s = \tan\left(\alpha + \frac{x}{2Ch}\right) \tan \pi x/s \tag{A1.20}$$

where α is the angle at which the field line meets the anode wire surface.

References

1. M.R. Spiegel, Theory and Problems of Complex Variables, Schaum McGraw-Hill, New York, 1964.
2. W.R. Smythe, Static and Dynamic Electricity, McGraw-Hill, New York 1950.
3. E. Kreyszig, Advanced Engineering Mathematics, Wiley, New York 1972.
4. H. Margenau & G.M. Murphy, The Mathematics of Physics and Chemistry, Van Nostrand, New York, 1956.
5. E. Weber, Electromagnetic Fields, Wiley, New York, 1950.

Appendix 2.

Derivation of single-wire formula

Fig. A2.1 represents schematically a single-wire chamber. The wire, and the grounded cathodes are normal to the $x-y$ plane. The cathodes are at $y=h$ and $y=-h$ and the wire is at complex coordinate position z_0.

(Before following the analysis below it may be helpful to examine first the preliminary section of Appendix 1.)

Consider the transformation

$$w = ie^{az} \tag{A2.1}$$

where $z = x+iy$, $w = u+iv$ and $a = \pi/2h$.
That is,

$$u = -e^{ax}\sin ay \tag{A2.2a}$$

$$v = e^{ax}\cos ay \tag{A2.2b}$$

It can be seen, therefore, that the line ABC at $y=h$ transforms into the negative u-axis while the line DEF at $y=-h$ transforms into the positive u-axis, as indicated in Fig. A2.1. All points between the cathodes map into the upper half-space in the w-plane.

We require to calculate the potential distribution $P(x,y)$ produced by a line charge of linear density q_0 at position z_0. Now it can be shown (ref. [1] of Appendix 1) that a harmonic function (one that satisfies Laplace's equation) remains harmonic under a conformal transformation. Thus, using the transformation A2.1, we need to find the complex potential function in the w-plane due to a line charge of density q_0 at w_0. This is a relatively simple problem that can be solved by use of an image line charge.

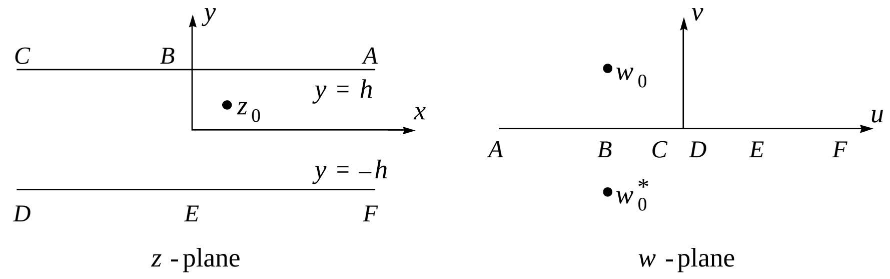

Figure A2.1

We first note that the real potential P at distance ρ from a single line charge in free space is of the form

$$P = \text{constant} - \frac{q_0}{2\pi\epsilon_0} \ln \rho \qquad (A2.3)$$

where ϵ_0 is the electrical space constant. Now the line charge is at w_0 and we wish to calculate the potential at a general point w distant ρ from w_0. That is

$$w = w_0 + \rho e^{i\gamma}$$

Then the complex potential function

$$W(w) = \text{constant} - \frac{q_0}{2\pi\epsilon_0} \ln(w - w_0)$$

has a real part equal to P, Eqn. A2.3.

Now if we place an image line charge density $-q_0$ at the complex conjugate position w_0^*, it is clear from symmetry considerations that the u-axis becomes a zero equipotential. The required complex potential function in the upper half-space of the w-plane becomes therefore

$$W(w) = -\frac{q_0}{2\pi\epsilon_0} \ln \frac{w - w_0}{w - w_0^*} \qquad (A2.4)$$

It now only remains to express the real and imaginary parts of this function in terms of x and y.

Firstly it is found after some manipulation that

$$W(z) = -\frac{q_0}{2\pi\epsilon_0} \ln \frac{\sinh a(z - z_0)/2}{\cosh a(z - z_0^*)/2} - i\frac{q_0}{2\pi\epsilon_0} a(z - z_0^*)/2$$

Then, if we write $W(z) = P(x,y) + iQ(x,y)$ it is found after further manipulation that

$$P(x,y) = -\frac{q_0}{2\pi\epsilon_0} \ln \left\{ \frac{\cosh\ a(x - x_0) - \cos\ a(y - y_0)}{\cosh\ a(x - x_0) + \cos\ a(y + y_0)} \right\}^{1/2} \qquad (A2.5)$$

and

$$Q(x,y) = -\frac{q_0}{2\pi\epsilon_0}(\theta + a y_0) \qquad (A2.6a)$$

where

$$\tan\theta = \frac{\sin ay - \cosh a(x - x_0)\sin a y_0}{\sinh a(x - x_0)\cos a y_0} \qquad (A2.6b)$$

Shift of the x-axis in the negative y-direction by an amount $d/2$, such that the upper cathode is at $y = h_1 = h + d/2$ and the lower cathode is at $y = -h_2 = -(h_1 - d/2)$ produces the more general result for the potential distribution in an asymmetrical chamber, Eqn. 4.1.

Appendix 3.
Derivation of cathode strip formula

We require to find the potential function due to a strip of the upper cathode, say between x_1 and x_2, being at unit potential, the remainder of that cathode and the lower cathode being grounded. The situation is shown in Fig. A3.1a.

In the following analysis it will be assumed that the preliminary section of Appendix 1 has been read. Further, the transformation to be used will be that employed in Appendix 2.

As described in Appendix 2, the line $y = h$ (the upper cathode) in the z-plane is mapped into the negative u-axis in the w-plane by the transformation

$$w = ie^{az} \tag{A3.1}$$

where $z = x + iy$, $w = u + iv$ and $a = \pi/2h$.
Thus

$$u = -e^{ax} \sin ay \tag{A3.2a}$$

$$v = e^{ax} \cos ay \tag{A3.2b}$$

The unit potential strip x_1, x_2 maps into the unit potential strip u_2, u_1 on the u-axis, Fig. 3.1b. It is now a relatively simple problem to determine the potential function in the w-plane.

Consider again a logarithmic function of the type employed in Appendix 2.

$$\begin{aligned} f(w) &= \ln(w - u_1) \\ &= \ln \rho_1 + i\theta_1 \end{aligned}$$

where ρ_1 is the distance between the points u_1 and w. Thus a valid complex potential function may be written.

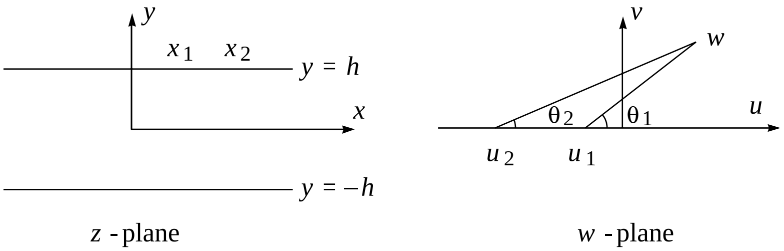

Figure A3.1

$$W(w) = A\ln(w - u_1) + B(w - u_2) + C$$

where A, B and C are constants to be determined by the boundary conditions. We now write

$$W(w) = Q(u, v) + iP(u, v) \tag{A3.3}$$

where Q and P are real functions of u and v, and in this case we regard Q as the flux function and P as the potential function. Thus

$$Q = A\ln\rho_1 + B\ln\rho_2$$

and

$$P = A\theta_1 + B\theta_2 + C$$

If $\theta_1 = 0$ and $\theta_2 = 0$ then $P = 0$. Therefore $C = 0$.
If $\theta_1 = \pi$ and $\theta_2 = 0$ then $P = 1$. Therefore $A = 1/\pi$.
If $\theta_1 = \pi$ and $\theta_2 = \pi$ then $P = 0$. Therefore $B = -1/\pi$.
Hence

$$P = (\theta_1 - \theta_2)/\pi \tag{A3.4}$$

and the potential function in the w-plane becomes

$$W = \frac{1}{\pi}\ln\left(\frac{w - u_1}{w - u_2}\right) \tag{A3.5}$$

It is convenient to derive an expression for the potential due to an infinitesimal cathode strip of width dx_2. That is, we need to find dP/dx_2 where

$$\frac{dP}{dx_2} = \frac{dP}{d\theta_2}\frac{d\theta_2}{du_2}\frac{du_2}{dx_2}$$

From Eqn. A3.4 $dP/d\theta_2 = -1/\pi$, and from Eqn. A3.2 $du_2/dx_2 = -ae^{ax_2}$. Further, from Fig. A3.1

$$\tan\theta_2 = v/(u - u_2)$$

Thus

$$\frac{dP}{dx_2} = \frac{a}{\pi}e^{ax_2}\frac{v}{(u - u_2)^2 + v^2}$$

Then, after further algebraic manipulation, it is found that

$$dP(x, y) = \frac{1}{4h}\frac{\cos ay}{\cosh a(x - x_2) - \sin ay}dx_2 \tag{A3.6}$$

If the x-axis in Fig. A3.1a is displaced in the negative y-direction so that it coincides with the lower cathode, and if the electrode separation $2h$ is replaced by the same symbol h, then Eqn. A3.6 becomes

$$dP(x,y) = \frac{1}{2h}\frac{\sin \pi y/h}{\cosh \pi(x-x_2)/h + \cos \pi y/h} dx_2 \qquad (A3.7)$$

This is the expression for potential employed in Section 6.2.2.

Appendix 4.
Evaluation of the exponential integral

If RC circuitry is employed in the processing of the signal from a coaxial counter or MWPC then a theoretical description will, inevitably, involve somewhere integrals of the type

$$I = \int_a^b \frac{e^z}{z}\, dz \tag{A4.1}$$

This has been demonstrated in Section 2.3 which describes a simple, standard signal processing system.

The integral A4.1 can be written

$$I = Ei(b) - Ei(a)$$

where $Ei(x)$ is the exponential integral [1]. A problem may arise in evaluating the integral A4.1 in the present applications because of the small value of the lower limit

$$a = t_0/T$$

where t_0 is the characteristic time of the chamber, $\leq 1\,\text{ns}$, Eqn. 2.10, and T is the RC processing time constant. If T is, typically, of the order $1\,\mu\text{s}$ then $a \leq 10^{-3}$. Under these conditions the numerical evaluation of A4.1 with normal library routines may yield an inaccurate result. The problem may be overcome as follows.

Choose a lower limit a', less than unity, but such that the integral of the type A4.1 can be evaluated with adequate accuracy ($a' = 0.1$, say, would be suitable).

That is

$$\begin{aligned} I &= \int_a^{a'} \frac{e^z}{z}\, dz + \int_{a'}^b \frac{e^z}{z}\, dz \\ &= I_1 + I_2, \quad \text{say.} \end{aligned}$$

In order to evaluate I_1 express the exponential as an expansion

$$\begin{aligned} I_1 &= \int_a^{a'} \frac{1}{z}\left(1 + z + \frac{1}{2!}z^2 + \frac{1}{3!}z^3 + \ldots\right) dz \\ &= \ln\left(\frac{a'}{a}\right) + \left[z + \frac{1}{2.2!}z^2 + \frac{1}{3.3!}z^3 + \ldots\right]_a^{a'} \end{aligned} \tag{A4.2}$$

The summation in Eqn. A4.2 can then be performed with a sufficient number of terms to reach the necessary accuracy.

I am grateful to Dr. J.R. Thompson, Mathematics Department, Leicester University, for pointing out this strategy.

Reference

1. M. Abramovitz & I.A. Stegun, Handbook of Mathematical Functions, Dover, New York, 1965.

Appendix 5.

The evaluation of $H_0(\omega)$ and $H(\omega)$

The account given below is a close reproduction of that originally given in ref. [1].

(1) It is prudent to begin with the evaluation of the simpler double sum for $H_0(\omega)$ which is, by Eqn. 5.20, $\sum_k s_k(\omega)$ where

$$s_k(\omega) = \sum_n 2\cos(\pi n) K_0 \left(2\omega \sqrt{c_k^2 + n^2} \right), \tag{A5.1}$$

and

$$4c_k^2 = (r_a/h)^2 + (ks/h)^2. \tag{A5.2}$$

The procedure here is to discover the equation

$$s_k(\omega) = 2\pi \int_0^\infty J_0(2\omega\gamma)\phi_k(\gamma)\gamma d\gamma, \tag{A5.3}$$

where

$$\phi_k(\gamma) = 1/[p_k \sinh(\phi P_k)],$$

and

$$p_k^2 = \gamma^2 + c_k^2.$$

This leads directly to

$$H_0(\omega) = 2\pi \int_0^\infty J_0(2\omega\gamma)\phi(\gamma)\gamma d\gamma, \tag{A5.4}$$

where

$$\phi(\gamma) = \sum_k \phi_k(\gamma). \tag{A5.5}$$

This is a convenient starting point for numerical evaluation of H_0 since the summation A5.5 may be closed around $k = \pm 10$, and the integral A5.4 may likewise be closed at an upper limit, γ_m say, around $\gamma = 4$. In both cases it is the sinh term in the denominator that accounts for the rapid convergence.

There is, however, one feature to which attention must be paid, which is the sharp spike in $\gamma\phi(\gamma)$ occasioned by the behaviour of $\gamma\phi_0(\gamma)$

around $\gamma = c_0$. Accordingly the term $\phi_0(\gamma)$ is replaced in the summation by $\phi_0(\gamma) - 1/(\pi p_0^2)$, which term should be evaluated using the series expansion

$$\frac{1}{t \sinh t} - t^{-2} = -\frac{1}{6} + \frac{7}{360}t^2 - \frac{31}{15120}t^4 + \ldots,$$

for values of πp_0 less than about 0.1. There remains the adjusting term

$$2\pi \int_0^{\gamma_m} j_0(2\omega\gamma)(1/\pi p_0^2)\gamma d\gamma,$$

which is equivalently

$$2\int_0^{\gamma_m} \frac{J_0(2\omega\gamma) - I_0(2\omega c_0)}{\gamma^2 + c_0^2}\gamma d\gamma + I_0(2\omega c_0) \ln \frac{\gamma_m^2 + c_0^2}{c_0^2}. \qquad (A5.6)$$

For values of $2\omega\gamma$ and $2\omega c_0$ both less than about 0.1, the last integrand may be evaluated by the series development

$$\frac{J_0(s) - I_0(t)}{s^2 + t^2} = -\frac{1}{4} + \frac{1}{64}(s^2 - t^2) - \frac{1}{2304}(s^4 - s^2t^2 + t^4) \ldots .$$

and otherwise by use of library routines.

It cannot be emphasised too strongly that the precautions suggested here are necessary if the integral A5.4 is to be evaluated correctly by numerical means; this is because of the smallness of c_0. Observe, too, that the choice of γ_m, which must be made consistently throughout, is determined by the behaviour of A5.4 and not that of A5.6.

(2) The derivation of Eqn. A5.3 from Eqn. A5.1 follows a technique that will be found in most texts on complex analysis. The terms for positive and negative n are combined, and by means of the calculus of residues one has

$$s_k(\omega) = 2K_0(2\omega c_k) - 2i \int \frac{K_0\left(2\omega\sqrt{c_k^2 + x^2}\right)}{\sin \pi x} dx,$$

where the path of integration in the complex x plane runs from $\infty + 0i$ parallel to the real axis, passes between the poles at $x = 0, 1$ and returns to $\infty - 0i$. This path may be displaced to the imaginary axis with indentations at $x = 0, \pm ic_k$; thereupon the change of variable $\gamma = i(c_k^2 + x^2)^{1/2}$ leads to

$$s_k(\omega) = 2K_0(2\omega c_k) - 2i \int K_0(-2i\omega\gamma)\phi_k(\gamma)\gamma d\gamma,$$

where the path of integration runs from $-\infty$ to ∞ passing above the pole at $\gamma = ic_k$. Capture of this pole gives a cancelling contribution $-2K_0(2\omega c_k)$, and there remains an integral along the real γ axis with an indentation above the origin that serves to fix the determination of $K_0(-2i\omega\gamma)$. Combining the contributions from each half of the axis into a single integral gives Eqn. A5.3.

(3) The evaluation of $H(\omega)$ follows the same course except that the transformation of the integral is more delicate. In particular, terms of opposite sign in k must be taken together to avoid problems with branch points. This argument is not given in detail. The problem with the spike in $\gamma\phi_0(\gamma)$ can be dealt with as before but the algebra is a little heavier.

In place of Eqn. A5.2 one defines

$$c_k = \text{abs }\ [(ks - z)/h]/2. \qquad (A5.2')$$

and, additionally,

$$Q_k(\gamma) = \frac{\sinh^2(\pi p_k)\cos(\pi y/2h)}{\sinh^2(\pi p_k) + \sin^2(\pi y/2h)}.$$

Then it may be shown that the formula parallel to Eqn. A5.5 is

$$\phi(\gamma) = \sum_k Q_k(\gamma)\phi_k(\gamma). \qquad (A5.5')$$

Again the $k = 0$ terms requires care when y and z are both small, and the technique employed above may be repeated since the factor $Q_k(\gamma)$ is well-behaved numerically. There is, however, the complication that the term exhibiting the logarithmic singularity,

$$2I_0(2\omega c_0)\int_0^{\gamma_m} \frac{1}{\gamma^2 + c_0^2} Q_0(\gamma)\gamma d\gamma \qquad (A5.7)$$

is not now directly integrable as it was earlier. Write

$$\begin{aligned} Q_0(\gamma) = & \frac{\pi^2 p_0^2 \cos(\frac{\pi y}{2h})}{\pi^2 p_0^2 + \sin^2(\frac{\pi y}{2h})} \\ & + \cos(\frac{\pi y}{2h}) \frac{\sin^2(\frac{\pi y}{2h})[\sinh^2(\pi p_0) - \pi^2 p_0^2]}{\Big[\sinh^2(\pi p_0) + \sin^2(\frac{\pi y}{2h})\Big]\Big[\pi^2 p_0^2 + \sin^2(\frac{\pi y}{2h})\Big]}, \end{aligned}$$

where p_0^2 is $\gamma^2 + c_0^2$. The first term leads at once in Eqn. A5.7 to the singular part

$$I_0(2\omega c_0)\cos(\pi y/2h)\ln\frac{\gamma_m^2 + c_0^2 + \sin^2(\pi y/2h)/\pi^2}{c_0^2 + \sin^2(\pi y/2h)/\pi^2},$$

and the second term may be integrated numerically with the numerator calculated by means of the series development

$$\sinh^2 t - t^2 = \frac{1}{3}t^4 + \frac{2}{45}f^6 + \frac{1}{315}t^8 \ldots,$$

when πp_0 is less than about 0.1.

Reference

1. J.R. Thompson, J.S. Gordon & E. Mathieson, Nucl. Instr & Meth. A234 (1985) 505.

Appendix 6.

Comments on gas gain formulae

The dependence of avalanche multiplication on chamber parameters and gas mixture properties is a complex topic, sufficiently so indeed to have received detailed study over nearly eighty years. An excellent, comprehensive description of this subject, particularly relevant to the present applications, has been given by Raether [1]. Several other detailed accounts of gas discharge physics may be found among them for example the very informative monograph by Llewellyn-Jones [2].

Not surprisingly no simple and accurate theory of gas gain in proportional detectors can be given. Nevertheless it is often necessary to have available empirical formulae to allow approximate predictions to be made of detector performance. There exist several such formulae, and it has to be accepted that no one formula is able to predict gain over the full range of operating voltage or over a complete range of chamber parameters. The purpose of this appendix is to outline briefly the essential features of the most useful of these empirical formulae.

The highly simplified theory underlying the establishment of a gas gain formula may be formulated as follows. Let $n(\ell)$ be the number of electrons in an avalanche at coordinate ℓ. Then the basic assumption, which ignores all secondary processes and space charge effects, is that the increase in number dn in an infinitesimal decrease in coordinate $-d\ell$ may be expressed as

$$dn = -\alpha n \, d\ell \tag{A6.1}$$

where here α is the Townsend first ionisation coefficient [1,2]. If one electron starts the avalanche at an average position ℓ_0 and the avalanche terminates at position ℓ_a, producing M electrons, then

$$\int_1^M \frac{dn}{n} = -\int_{\ell_0}^{\ell_a} \alpha d\ell$$

or

$$\ln M = \int_{\ell_a}^{\ell_0} \alpha d\ell \tag{A6.2}$$

The different empirical formulae arise from the various forms assumed for the dependency of α on field E.

Fig. A6.1 sketches the general way in which α/p depends on $S = E/p$, where p is the gas pressure (general considerations show that α/p is a function of E/p).

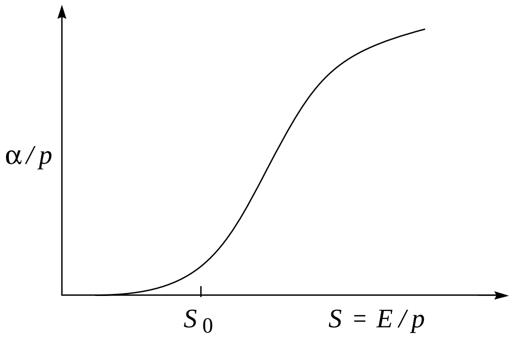

Figure A6.1

At low values of α/p, such as would be used in PPACs, the original Townsend form [1,2] is often employed.

$$\alpha/p = ae^{-b/S}$$

where a and b are constants. This form has also been assumed for coaxial counter operation by Williams and Sara [3] to obtain a gas gain formula.

At higher values of α/p there is a fairly well-defined linear region. Diethorn [4] has assumed direct proportionality with S to obtain a coaxial counter gain formula. Zastawny [5,6] has employed the more realistic form over the linear range

$$\alpha/p = B(S - S_0) \qquad (A6.3)$$

where B and S_0 are constants. Zastawny has included a further constant to take into account the non-linear region as α/p approaches zero. A simplified analysis, based on Eqn. A6.3 only, will be given below.

Rose and Korff [7] developed a semi-empirical theory to determine the form of α/p, finding proportionality with $S^{1/2}$

Finally, (not in chronological terms) Khristov [8] has obtained a coaxial counter gain formula based on α/p equal to a constant.

The Zastawny description [5] appears to be the most accurate of these various empirical formulae. A simplified, two-parameter analysis may be developed as follows, using the symbols and formulae employed in Chapter 2. For a coaxial counter

$$S = \frac{E}{p} = \frac{2CV_a}{pr}$$

and therefore

$$dr = -\frac{2CV_a}{pS^2}\,dS$$

Thus Eqn. A6.2 may be written

$$\ln M = 2CV_a \int_{S_0}^{S_a} \left(\frac{\alpha}{p}\right) \frac{dS}{S^2}$$

where $S_a = 2CV_a/pr_a$. Hence, from Eqn. 6.3,

$$\ln M = 2CV_a B\{\ln(r_0/r_a) - 1 + r_a/r_0\} \qquad (A6.4a)$$

where

$$r_0 = 2CV_a/pS_0 \qquad (A6.4b)$$

Eqn. A6.4 is an extremely useful, if approximate, expression for estimating changes of gain with chamber geometry, pressure or operating voltage (see, for example, 3.5.3). It is of course equally applicable to multiwire chambers, at normal operating pressures, provided the appropriate value of C is employed (Section 4.3.2).

The logarithmic slope, employed during the study of gain dependence on count rate (Section 3.6) is given by

$$\frac{1}{M}\frac{dM}{dV_a} = 2CB \ln\left(\frac{2CV_a}{S_0 p r_a}\right)$$

The near independence of this slope from V_a, over a limited range, is demonstrated here.

Some experimental values of the two parameters B and S_0 are given in the table below.

Gas	$B(\mathrm{kV})^{-1}$	S_0(V/cm torr)
CO_2 [5]	19.3	69
Ar/10%CH_4 [5]	30	25
Ar/20%CO_2 [9]	23	18
Xe/10%CO_2 [9]	27	28

References

1. H. Raether, Electron avalanches and breakdown in gases, Butterworths, London, 1964

2. F. Llewellyn-Jones, Ionisation and breakdown in gases, Methuen, London, 1966
3. A. Williams & R.I. Sara, Int. J. Rad. & Isotop., 13(1962) 229
4. W. Diethorn (see R.W. Hendricks, Nucl. Instr & Meth. 101 (1972) 309 and G.F. Knoll, Radiation Detection and Measurement, Wiley, New York, 1979)
5. A. Zastawny, J. Sci. Instr. 43 (1966) 179.
6. A. Zastawny, J. Sci. Instr. 44 (1967) 395.
7. M.E. Rose & S.A. Korff, Phys. Rev. 59 (1941) 850.
8. L.G. Kristov, Dokl. Bulg. Akad. Nauk. 10 (1947) 453.
9. G.C. Smith (private communication), Brookhaven National Laboratory.

Appendix 7.

Prompt electron signal in wire chambers

In the wire chamber calculations in this monograph it has been assumed that the final stages of the avalanche occur so close to the anode wire surface that the electron component of the anode signal is negligible. This appendix will show that under normal operating conditions, this assumption can be completely justified quantitatively. In this analysis it will be assumed that the electrons in the avalanche are collected in zero time and that space charge effects can be ignored.

Let dn be the number of ions (and electrons) created in the interval dr. Then the net anode charge, due to electron collection and positive ion creation, is (Eqn. 2.6.)

$$dq_e = -ednC\ln(r/r_a)^2$$

where $-e$ is the electronic charge. Thus the total net anode signal, immediately after the avalanche, becomes

$$q_e = e2C\int_{r_a}^{r_0}\ln\left(\frac{r}{r_a}\right)\frac{dn}{dr}\,dr \qquad (A7.1)$$

Here r_0 is the radius at which gas multiplication starts, that is where $n = 1$. The total avalanche charge is $q_0 = eM$ where M is the gas gain. Then, integrating by parts Eqn. A7.1, we find

$$\frac{q_e}{q_0} = -\frac{2C}{M}\int_{r_a}^{r_0}\frac{n-1}{r}\,dr \qquad (A7.2)$$

We cannot proceed further analytically with this problem. A particular gain formula must be employed to represent $n(r)$ and no reasonable choice allows Eqn. A7.2 to be integrated analytically.

An extremely useful and simple gain formula is the modified Zastawny formula described in Appendix 6. In this formulation $n(r)$ is obtained from the equation

$$\ln n(r) = 2CBV_a\{\ln(r_0/r) - 1 + r/r_0\} \qquad (A7.3)$$

where B and r_0 have been introduced in Appendix 6. The value of M is obtained from Eqn. A7.3 by placing r equal to r_a. If $n(r)$ from Eqn. A7.3 is employed in Eqn. A7.2, and the integration performed numerically, then it is found that, for the normal range of chamber operating geometries and conditions, $-q_e/q_0$ falls within the range 1 to 5%.

It should be stressed that this last result represents the abrupt jump in anode charge immediately after the avalanche. The resultant change in output amplitude, after signal processing, is very much smaller than this and is quite negligible, under normal operating pressure conditions. This can be appreciated by recalling the extremely fast rise of the anode charge waveform. Eqn. 2.12 shows that at $t = 0$

$$\frac{dq_e}{dt} = -\frac{q_0 C}{t_0}$$

where t_0 is the chamber characteristic time (0.3–1.0 ns). Thus the sudden step $-q_e/q_0$ represents a shift of the charge waveform, in the negative time direction, by an amount Δt given by

$$\Delta t = -\frac{t_0}{C}\frac{q_e}{q_0}$$

Since, for wire chambers and coaxial counters, C falls within the range 0.04 to 0.1 approximately it is seen that the effective time shift of the charge waveform, under normal operating pressure conditions, is a fraction of a nanosecond. The effect of this shift on pulse height, even with the fastest signal processing, is negligible.

Finally, it may be noted here that the effect of finite collection duration would generally be very much greater than this present effect of positive ion position. A simple extension of the analysis of Section 2.3 shows that a primary spread of only a few nanoseconds can result, with the fastest available processing systems, in a significant, measurable change in pulse height.